ACS NANO

www.acsnano.org

PERSPECTIVE

Quo Vadis, Nanoparticle-Enabled *In Vivo* Fluorescence Imaging?

Erving Ximendes, Antonio Benayas, Daniel Jaque,* and Riccardo Marin*

Cite This: *ACS Nano* 2021, 15, 1917–1941

Read Online

ACCESS | Metrics & More | Article Recommendations

ABSTRACT: **The exciting advancements that we are currently witnessing in terms of novel materials and synthesis approaches are leading to the development of colloidal nanoparticles (NPs) with increasingly greater tunable properties. We have now reached a point where it is possible to synthesize colloidal NPs with functionalities tailored to specific societal demands. The impact of this new wave of colloidal NPs has been especially important in the field of biomedicine. In that vein, luminescent NPs with improved brightness and near-infrared working capabilities have turned out to be optimal optical probes that are capable of fast and high-resolution *in vivo* imaging. However, luminescent NPs have thus far only reached a limited portion of their potential. Although we believe that the best is yet to come, the future might not be as bright as some of us think (and have hoped!). In particular, translation of NP-based fluorescence imaging from preclinical studies to clinics is not straightforward. In this Perspective, we provide a critical assessment and highlight promising research avenues based on the latest advances in the fields of luminescent NPs and imaging technologies. The disillusioned outlook we proffer herein might sound pessimistic at first, but we consider it necessary to avoid pursuing "pipe dreams" and redirect the efforts toward achievable—yet ambitious—goals.**

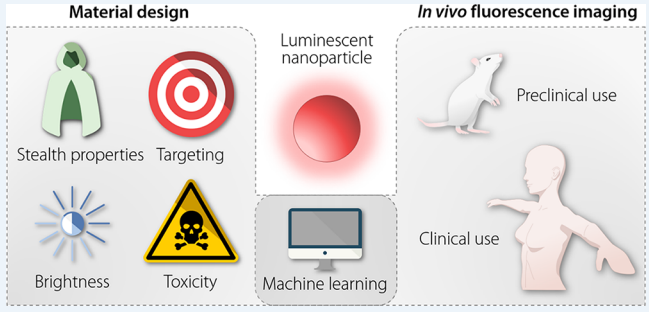

Optical imaging techniques make use of light[1]—matter interactions to extract information about biological systems. This family of diagnostic approaches generates contrast in images by capitalizing on different physical mechanisms involving light, such as scattering,[2] absorption,[3−5] conversion to heat,[6] and photoluminescence.[7,8] Although endogenous tissue components often already provide optical signals, exogenous materials (*i.e.*, contrast agents) are frequently introduced in the biological system to increase contrast.[9−11] The search for suitable contrast agents is a major driver in nanomedicine, along with the development of new approaches capable of localized therapy. These two subfields seamlessly merge in the research area of theranostics, wherein nanoparticles (NPs) that combine therapeutic and diagnostic properties are targeted.[12,13] Whether executed with a theranostic or a contrast agent, the initial step of disease imaging is pivotal to direct the therapeutic efforts and to minimize side effects on healthy tissues.[14] Therefore, the development of NPs meeting the requirements of an ideal contrast agent is key. One question arises though: *What are the requirements of an ideal contrast agent?* A clear answer to that question provides an approach to the issue of preparing contrast agents with real potential to be implemented in the clinic. In this Perspective, we attempt to answer that question, drawing inspiration from recent publications on the use of inorganic NP-based contrast agents for *in vivo* fluorescence imaging. In doing so, we highlight the latest trends in the field while also pinpointing exciting challenges that lie ahead. Although our discussion focuses on a specific category of contrast agents (inorganic luminescent NPs), many general considerations concerning toxicity and selectivity can be extended to any NP to be used in the biomedical realm. Our hope is that the critical assessment of the state-of-the-art presented in this Perspective will support the evermore thought-out design of NP-based contrast agents. This process entails moving away from some common misconceptions as well as implementing methodologies that will enable a smoother transition toward use by physicians. Finally, we identify the fields where NP-supported fluorescence imaging applications can have a real impact (both at clinical and preclinical stages)—a necessary and disillusioned appeal to

Published: January 19, 2021

https://dx.doi.org/10.1021/acsnano.0c08349
ACS Nano 2021, 15, 1917–1941

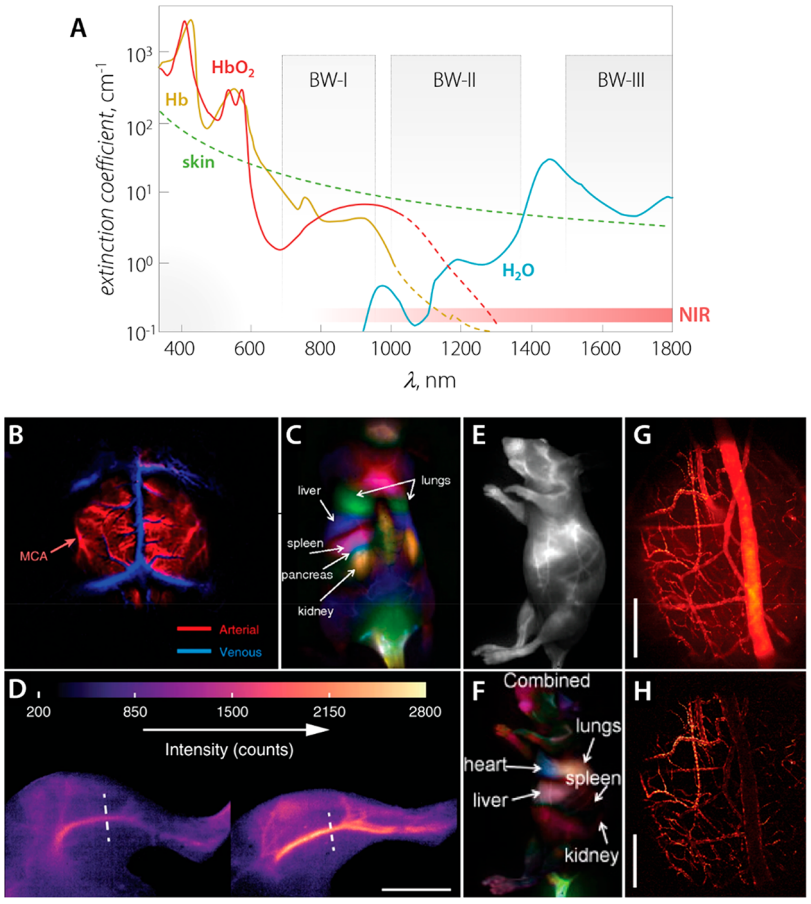

Figure 1. The three biological windows and fluorescence anatomical imaging with near-infrared-emitting nanoparticles. (A) The three biological windows (BWs) all fall in the near-infrared (NIR) wavelength range and are delimited by the optical properties of several tissue components. The absorption of water and hemoglobin (oxygenated HbO_2 and deoxygenated Hb) is shown along with the scattering from skin. The overall extinction that results from the combination of light absorption and scattering from these components (and others) frames three wavelength ranges known as biological (or optical transparency) windows: BW-I, 750−950 nm; BW-II, 1000−1350 nm; and BW-III, 1500−1800 nm. Note that the limits of the BWs are not strictly defined, and often different numbers are reported. The best performance for luminescence imaging contrast agents have been obtained so far with nanoparticles (NPs) that are excited in BW-I and whose emission falls in BW-II. In (B−H), different anatomical fluorescence images acquired using NIR-emitting NPs are presented. (B) Cerebral vascular image in the BW-III region with corresponding principal component analysis (PCA) overlaid showing arterial (red) and venous (blue) vessels of a C57Bl/6 mouse with Er-doped rare-earth-based NPs. Reprinted with permission from ref 34. Copyright 2017 Springer Nature. (C) Dynamic contrast-enhanced imaging with CNTs through PCA. Major features observed belong to the lungs, liver, kidneys, and spleen. Reprinted with permission from ref 28. Copyright 2011 PNAS. (D) BW-II fluorescence images (background-corrected) of the left hind limbs of two mice immediately after intravenous injection of Ag_2S dots (left) or Ag_2S superdots (right). Reprinted with permission from ref 35. Copyright 2020 Springer Nature. (E) BW-II/BW-III fluorescence image of blood flow in the nude mouse after injection of PEGylated Ag_2S quantum dots (QDs) and (F) the corresponding PCA. Reprinted with permission from ref 36. Copyright 2014 Elsevier. (G,H) High-resolution, high-speed multicolor angiography images of a glioblastoma tumor through a cranial window using QDs composite NPs. Reprinted with permission from ref 37. Copyright 2017 Springer Nature.

reason, mainly enforced by the intrinsic physical constraints of the technique.

FLUORESCENCE IMAGING: FUNDAMENTALS, ADVANTAGES, AND DRAWBACKS

Fluorescence imaging is based on the detection of the electromagnetic radiation within the ultraviolet-visible-near-infrared (UV-vis-NIR) range that is emitted by either tissues or exogenous elements. It is used to build up images of cells, tissues, and animals. Although the autofluorescence of tissues can be used itself for bioimaging, it lacks specificity as different tissues usually show very similar emission spectra, which are located for the most part within the visible range.[15,16] In addition, the fast attenuation of autofluorescence, caused by the large optical extinction of tissues in the visible range, hampers its use for deep-tissue and whole-body anatomical imaging.[17,18] Alternatively, fluorescence imaging is made possible by introducing optical probes (contrast agents) that can be excited by light into the specimen to be visualized.[19] The use of this low-energy excitation radiation avoids the intrinsic risks associated with ionizing radiation (mainly alterations of DNA structure).[20] The use of suitable contrast agents improves the performance of the different fluorescence imaging modalities, which can be distinguished depending on their specific biomedical aim: anatomical, functional/metabolic, or molecular imaging.[21]

If opting to use an exogenous contrast agent, the properties of this optical probe should be tailored to the needs of the specific application. In addition to the use of non-ionizing radiation, fluorescence imaging offers relevant advantages over other imaging technologies such as magnetic resonance imaging

https://dx.doi.org/10.1021/acsnano.0c08349
ACS Nano 2021, 15, 1917−1941

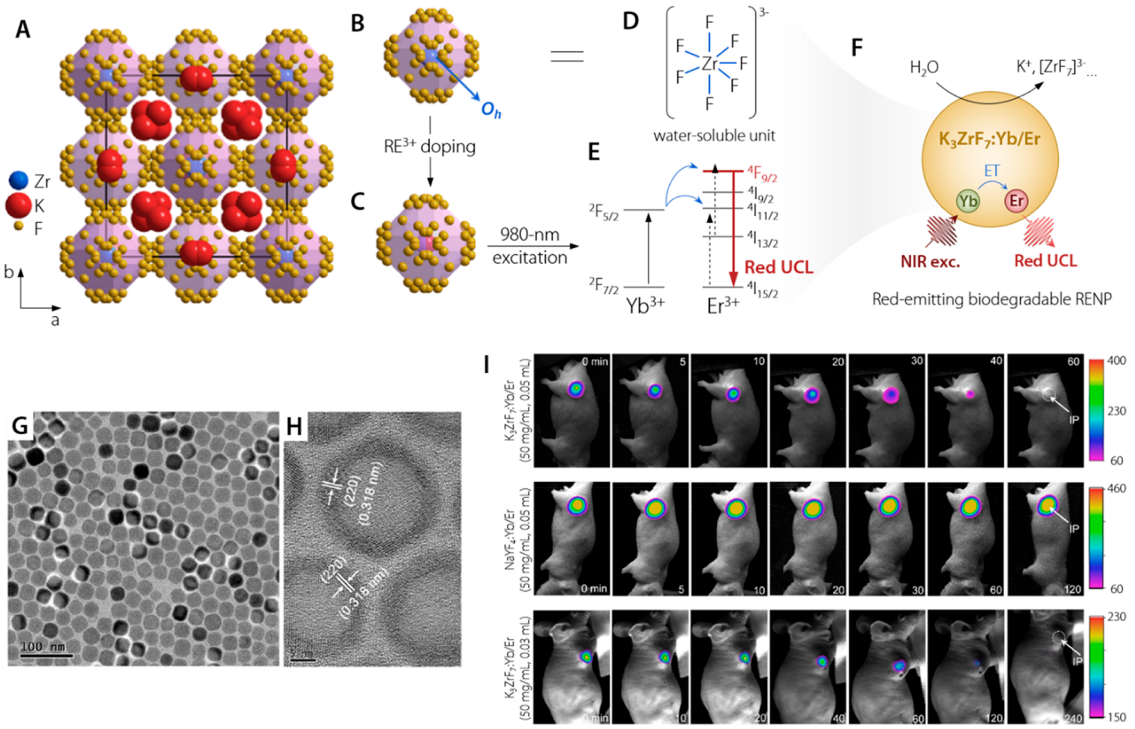

Figure 2. Soluble K_3ZrF_7:Yb^{3+}/Er^{3+} nanoparticles (NPs) for fluorescence imaging. Crystal structure of (A) K_3ZrF_7 and (B) single $[ZrF_7]^{3-}$ unit, wherein Zr^{4+} occupies a site with O_h coordination environment. (C) Doped RE^{3+} ions substitute in this site Zr^{4+}. Salient characteristics of the K_3ZrF_7:Yb^{3+}/Er^{3+} NPs are (D) the presence of the water-soluble $[ZrF_7]^{3-}$ unit and (E) an almost pure red upconversion luminescence under 980 nm excitation. (F) Combined, these features make these NPs excellent candidates for fluorescence imaging. (G) Transmission electron microscopy observation shows a sample highly monodisperse in size with (H) good crystallinity. (I) The *in vivo* dissolution of the NPs after subcutaneous administration was followed by monitoring the emission intensity *versus* time and comparing it to the trend observed for $NaYF_4$:Yb^{3+}/Er^{3+} NPs. Adapted from ref 38. Copyright 2020 American Chemical Society.

(MRI), nuclear imaging (*e.g.*, positron emission tomography, PET), or computed tomography (CT) as well: the possibility of real-time imaging and the reduced cost of required equipment. Indeed, fluorescence imaging "simply" requires a fluorescence camera for image acquisition and a laser source for excitation of the tissue or the exogenous contrast agent.

Among the different contrast agents for fluorescence imaging currently being investigated (small molecules, aptamers, antibodies, peptides, *etc.*), inorganic fluorescent NPs (from now on simply fluorescent NPs) offer a broad palette of assets.[22] It is feasible to engineer their different physicochemical characteristics and to attach diverse functional groups to their surface.[23] Moreover, their small sizes (below 100 nm) enable them to navigate through the bloodstream and to enter different organs and tissues, even being taken into cells. Fluorescent NPs can absorb the excitation light and re-emit it in a different spectral range. If the NP emission spectrum is significantly different from that of the tissue's autofluorescence, the fluorescence image can provide reliable information about the locations of NPs (with some important caveats that we discuss below).[24,25] Furthermore, the intensity and contrast of the fluorescence image can provide information about the local density of the contrast agent. There are a plethora of luminescent NPs that have been used for *in vivo* fluorescence imaging.[19] Among them, some of the most relevant results have been obtained by using rare-earth-based NPs (RENPs), semiconductor nanocrystals ((among them, quantum dots; QDs)), and carbon-based nanostructures such as carbon dots (CDs) and carbon nanotubes (CNTs). The best results have been obtained when the operating ranges (excitation/emission wavelengths) of these NPs were tuned to fall within the three NIR biological windows (spectral ranges between 750 and 1800 nm, where tissues are partially transparent to electromagnetic radiation; see Figure 1).[26,27] Hence, it is relevant to underscore that NIR-emitting RENPS, CNTs, and QDs were shown to afford *in vivo*, high-resolution, and high-contrast whole-body anatomical imaging in small animal models.[28−31] However, we should be realistic: Not all the characteristics of luminescence imaging are advantageous, particularly targeting *in vivo* applications. The most troublesome one has the form of the Beer−Lambert law. This law describes the extinction of light in a medium as an exponential function, which is even more accentuated through optically dense biological tissues (in both the excitation and emission paths). This extinction entails scattering and absorption of photons. As a result, the penetration depth achievable with fluorescence imaging inside biological tissues is greatly limited, both in comparison with previously mentioned imaging modalities (*i.e.*, MRI, PET, CT) and with optical imaging methods relying on the synergy between diffuse light (scattered) and advanced processing techniques.[32] Therefore, even for small animals, infrared fluorescence imaging-based tomography for the acquisition of three-dimensional (3D) images of sufficient resolution appears to be a distant dream, although first steps are being taken.[33] Yet, in the context of contrast-agent-based fluorescence imaging, working in parallel on the fronts of increasing the brightness of the contrast agent's fluorescence signal and its spectral position, a sizable increase in the achievable penetration depth has been witnessed in recent years (*vide infra*).

https://dx.doi.org/10.1021/acsnano.0c08349
ACS Nano 2021, 15, 1917−1941

DEGRADABLE NANOPARTICLES: ADVANCES TOWARD ZERO TOXICITY

This Perspective was inspired by the paper by Liu, Hong, and co-workers in the December 2020 issue of *ACS Nano*, which reports RENPs with higher solubility in biological environments compared to canonical RENPs such as $NaYF_4$-based NPs (Figure 2).[38] $NaREF_4$ NPs are known to undergo degradation upon exposure to aqueous media containing phosphate groups, particularly at low NP concentrations.[39−42] The RENPs reported by Liu, Hong, and colleagues are composed of K_3ZrF_7, a material whose "soft" crystal lattice imparts superior water solubility to the system. Indeed, the lattice features $[ZrF_7]^{3-}$ units and K^+ ions as building blocks that can be easily solubilized by water. The distorted pentagonal-bipyramidal coordination environment with O_h site-symmetry experienced by Zr^{4+} offers a favorable site for RE^{3+} substitution, given its high coordination number. In the structure, the 7 F^- anions occupy >100 dynamically equivalent positions, a situation that possibly underscores a "fluidity" of the lattice and a high tolerance to defects. In fact, RE^{3+} ions can be doped at high concentration in the structure despite the charge and size mismatch with Zr^{4+}, which is bound to introduce anion vacancies in the lattice upon substitution. Both NIR-emitting ions (Nd^{3+}/Yb^{3+}) and the iconic upconverting pair Yb^{3+}/Er^{3+} can be doped in the structure, thus yielding downshifting or upconversion emission under NIR excitation within biological window (BW)-I and BW-II. Importantly, both high and low pH values prompt dissolution of the RENPs at a fast rate: A behavior observed also after the dispersion of the hydrophobic RENPs in peanut oil and subcutaneous injection in mice. The authors followed the dissolution within animals spectroscopically as well as *via* mass spectroscopy on collected excretions and harvested organs. They observed almost complete excretion of the solubilized material, which dramatically reduces the risk of toxicity due to accumulation of particles or ions (Zr^{4+} in this case) at specific organs, such as lungs and liver. At the same time, the upconversion emission was observed up to 2 h post-injection, a time span sufficient to perform imaging. Despite the relevance of the results published by Liu, Hong, and co-workers, the potential application of their visible emitting NPs for *in vivo* imaging is limited due to the strong tissue extinction in this spectral range (Figure 1A). This limitation could easily be overcome by an adequate choice of RE ions. For example, as already proposed by the authors of the study, one can move from the Er/Yb pair to Nd/Yb to enable shifting the emission wavelength from the visible to BW-II. This alteration yields a nanostructure capable of deep-tissue, *in vivo* imaging that is soluble in biological environments.

These RENPs, which diligently vanquish after they have done their job as contrast agents, constitute a step in the right direction for future research efforts on fluorescence imaging for *in vivo* applications. Indeed, these RENPs address one main concern linked to the use of NPs in biomedicine generally speaking, namely their long-term toxicity owing to accumulation in organs.[43]

Achieving dissolution of the NPs is one way to approach the issue of accumulation. However, this strategy only works for NPs whose dissolution products exhibit negligible toxicity. Most of the NPs investigated for biomedical applications are far less soluble in biological media and/or are composed of materials that can be leached into potentially cytotoxic ions (*e.g.*, Ag^+ and Cu^{2+}).[44,45] Moreover, an extended circulation time is usually required to enable NP accumulation at the tissue of interest (to be imaged or treated). Strategies have been developed to design stealthier (*i.e.*, biomimetic) NPs to avoid premature uptake from macrophages (*vide infra*). In those cases, it is beneficial to limit the NP dissolution further (*via* suitable surface coatings) and rely on their clearance. Intravenously administered NPs usually undergo elimination mainly *via* renal (smaller NPs, < 5.5 nm) and hepatobiliary elimination (larger NPs).[46,47] The former mechanism is better understood than the hepatobiliary pathway; thus, future efforts should be devoted to increase our understanding of the complex mechanisms underpinning the latter. To that end, Chan and co-workers recently investigated the barriers encountered by model Au NPs of different sizes during hepatobiliary elimination after intravenous injection (Figure 3).[48] Combining their results with previous literature,

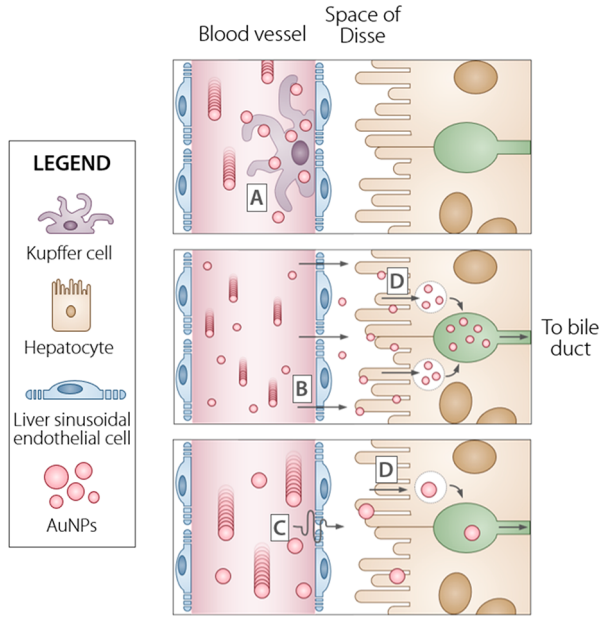

Figure 3. Mechanism of hepatobiliary elimination for nonsoluble nanoparticles (NPs) in the liver sinusoid proposed by Chan and co-workers.[48] The authors suggest that, after intravenous injection, the NPs enter the liver and are subsequently taken up by Kupffer cells in the liver sinusoid (A). The larger circulating NPs are sequestered more easily, whereas smaller NPs cross the sinusoidal endothelium (B). Upon removal of the Kupffer cells, the larger NPs can also more easily extravasate. However, the fenestrae size limit of the liver sinusoidal endothelial cells can hinder this process (C). Lastly, the NPs accumulate at the space of Disse, where hepatocytes take them up, favoring the NP transport into the bile canaliculus (D). The final step is constituted by the transit of the NP outside the liver and into the intestine, from where they are eventually expelled from the body through the feces. Adapted from ref 48. Copyright 2019 American Chemical Society.

they highlighted the prominent role played by Kupffer and liver sinusoidal endothelial cells in reducing the effectiveness of this form of NP excretion. The authors observed that both types of cells are capable of strongly interacting with NPs due to their high phagocytic ability toward the NPs. In order to enhance clearance through this hepatobiliary elimination, NPs should therefore be engineered to minimize the interaction with these cells, which constitute the first line of defense of the liver.

https://dx.doi.org/10.1021/acsnano.0c08349
ACS Nano 2021, 15, 1917−1941

CHARACTERISTICS OF A NANOPARTICLE-BASED FLUORESCENCE IMAGING CONTRAST AGENT

In a more holistic way, there are several points to consider when designing NPs for biomedical use, some of which are specific to the case of NP-based fluorescence imaging contrast agents. To

> This Perspective was inspired by the paper by Liu, Hong, and co-workers in the December 2020 issue of *ACS Nano*, which reports rare-earth nanoparticles (RENPs) with higher solubility in biological environments compared to canonical RENPs such as $NaYF_4$-based NPs.

that end, in this Perspective, we identify the following aspects as the most important ones to take into account for future experimental efforts in the field.

- Toxicity: This is a rather broad and multifaceted issue, and control over it requires attention to the composition of the constituent material, NP surface chemistry, and size/morphology.
- Stealth properties: The NPs should elude the lines of defense of the organism, residing within the body long enough to accumulate at the site of interest rather than being prematurely cleared.
- Specificity: The NPs should bind as specifically as possible to the targeted tissue, aiming for a "magic bullet"-like type of properties and overcoming possible physical barriers within the body.
- Range of excitability and emission: Light of specific wavelengths interact less with the constituents of tissues, thus affording deeper penetration within the human body as well as less spectral distortion.
- Brightness: The more photons that are emitted per photons shined on the NP, the more effective the contrast agent will be because it can afford higher penetration depth, contrast, and resolution (both spatial and temporal).

The next sections will specifically deal with these aspects, reviewing those we believe have been highlights in past years and suggesting future directions of investigation.

Minimizing Toxicity and Immune Response while Enhancing Specific Targeting. Human beings did not invent NPs. In nature, they can be found in dust, sand, volcanic ash, and even in some biological entities such as magnetotactic bacteria or viruses (which are nanosized themselves).[49−52] However, anthropogenic activity has led to an increased presence of NPs in the environment, which translates to heavier exposure to a greater variety of materials. Before the era of nanotechnology, NPs were grouped with larger submicrometric materials in the broader category of ultrafine particles (UFPs), a term still used in toxicology to refer to this class of tiny materials. Therefore, although the term nanotoxicology appears in the literature between the years 2003/2004,[53−55] concerns and studies about the effect of NPs (or UFPs) on health predate the coinage of this word.[56−59] Exposure to NPs in nature mainly occurs *via* inhalation, and from the tissue of the upper and lower respiratory tract, the NPs can enter the bloodstream and/or translocate to other systems.[60−62] NPs can also enter the body *via* skin contact (*e.g.*, sunscreen) and oral ingestion, and the advent of nanomedicine will result more consistently in the direct injection of NPs into the body.[63] The latter exposure route is the one most likely to be of interest in the framework of fluorescence imaging for *in vivo* applications and has been shown to pose higher risks connected to NP accumulation.[64] Importantly, once the NPs are in the bloodstream and/or accumulated at the site of interest, they can elicit an immune response. This side effect is to be avoided, but what are the features of NPs that play a role in this context? In the past couple of decades, several studies have highlighted the effects of NP composition, size, morphology, and surface chemistry/charge in the human body (Figure 4). Before delving into these aspects, it

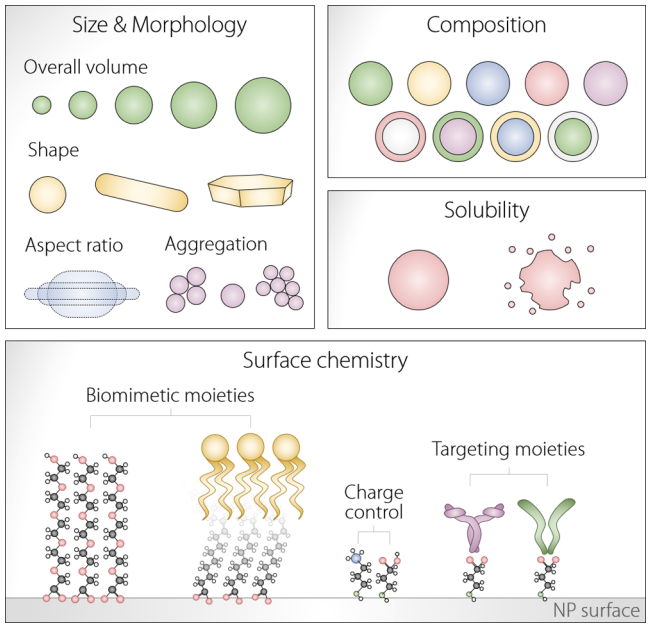

Figure 4. Summary of the most relevant parameters for the toxicity of nanoparticles (NPs). This summary is not intended to be comprehensive but rather to provide the reader at a glance with the most important aspects that influence NP toxicity and, more generally, the interactions between NPs and biological entities.

is important to mention that it is not always easy to investigate their effects separately, owing to the difficulty in carrying out such investigations *ceteribus paribus* (*i.e.*, all other conditions fixed).[64] Controlling particular variables is somewhat possible within the framework of a single study; however, it is almost impossible to compare the results obtained in different investigations carried out around the world due to the lack of standardization in nanomaterial toxicity assessments and the inherent difficulty in controlling the properties of nanomaterials on a batch-to-batch scale in a fully reproducible way. Setting standards in terms of procedures and parameters reported in each study is of utmost importance to advance the knowledge in the field of nanobiotechnology.[65−67] To that end, Caruso, Crampin, and co-workers have already proposed guidelines for minimum information reporting in bio−nano experimental literature, openly encouraging "the bio−nano science community to adopt a "reporting standard" to enhance the quality and reuse of published research".[68] Following such guidelines should become the praxis for a more impactful and relevant advancement of our knowledge.[69] We argue that efforts to screen for

https://dx.doi.org/10.1021/acsnano.0c08349
ACS Nano 2021, 15, 1917−1941

compliance to this good practice at the editorial level will also be most beneficial in this regard.

Before discussing NP toxicity, stealth properties, and targeting ability in more detail, we should point out how the use of artificial intelligence (AI) is emerging as a powerful tool to predict the toxicity[64,70] and fate[71] of NPs possessing different compositions, sizes, morphologies, and surface chemistries (Figure 5). The use of these neural networks requires large amounts of data as a training set to then be able to predict the behavior of a NP reliably. Therefore, the identification of a minimum set of parameters to be provided in studies focusing on the biomedical application of NPs (and that can be used to feed the learning algorithm) is key to support the advancement of this predictive tool. As we detail further toward the end of this Perspective, we believe that the contribution of AI to the future of luminescence imaging does not end here.

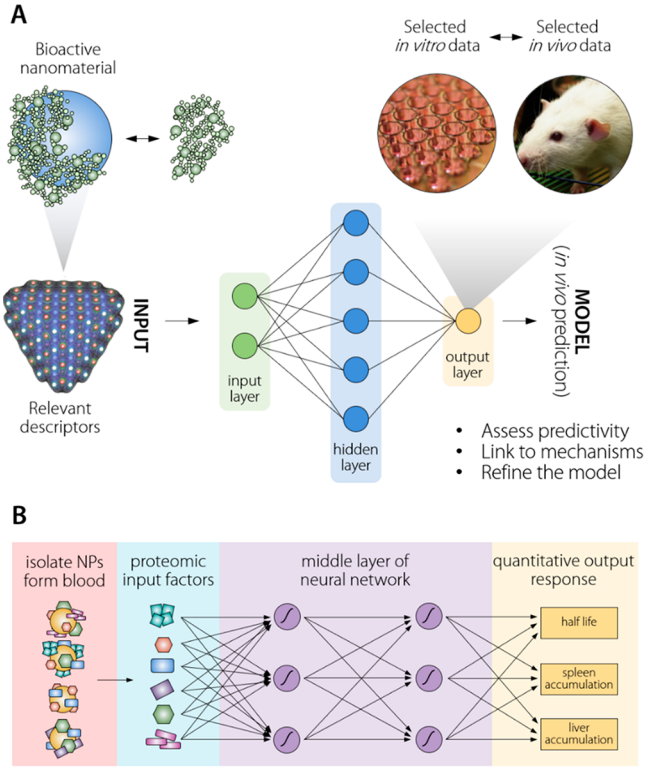

Figure 5. Artificial intelligence to predict the toxic effect and fate of nanoparticles (NPs). (A) Scheme of the quantitative structure–activity relationship method as summarized by Winkler *et al.*[70] The most relevant molecular descriptors of the bioactive form of nanoparticles (NPs; *i.e.*, coated with biological molecules upon interaction with the environment) are identified. The neural network is trained with this input of descriptors, along with *in vivo* and/or *in vitro* data. These data sets can also be used to generate a statistical regression model. Using the validated model, the properties of new nanomaterials can be predicted as well as biological mechanisms and processes. Reprinted with permission from ref 70. Copyright 2013 Elsevier. (B) Scheme of the approach developed by Lazarovits *et al.* for the prediction of the fate of NPs *in vivo*.[71] After intravenous injection of different Au NPs in mice, the NPs were isolated from blood and the proteins adsorbed on the surface identified and quantified *via* mass spectrometry. These data were used to train the neural network along with quantitative information on the accumulation of the NPs at different organs (also obtained *via* mass spectrometry). After training and validation, the neural network could predict the behavior of unknown NPs. Adapted from ref 71. Copyright 2019 American Chemical Society.

Chemical Composition. Since 2003, Europe has banned heavy metals from most vehicle components,[72] and an extension of this ban to electronic devices has been on the table for a long time.[73] Along with mercury and hexavalent chromium, cadmium and lead are on the blacklist; coincidentally, they are among the most used metals for producing highly efficient QDs. Cd-based QDs are the benchmark in terms of luminescence intensity in the visible part of the spectrum, with photoluminescence quantum yields (PLQYs, number of emitted photons per number of absorbed photons) approaching unity.[74] PbS QDs, particularly in their PbS/CdS core/shell form, are uniquely interesting for *in vivo* biomedical applications owing to their brightness and NIR working capabilities, which ensure better penetration depth (*vide infra*).[75] Admittedly, exceptions to the ban have been introduced, due to technological limitations that prevent obtaining the same standards achievable with materials and processing techniques involving heavy metals.[76] However, it is natural to think that if heavy-metal-containing QDs have an uncertain future in several technological fields, it is highly unlikely that similar NPs will work their way into clinical practice. One of the main issues is in the possibility of metal ion leaching within the body. One might argue that the total amount used is generally small (see Table 1), hence, the benefit of accurate detection leading to a reliable diagnosis should greatly outweigh the risks associated with the toxicity of the contrast agent. However, at times it is necessary to repeat the imaging procedure more than once to assess the development of the disease or the efficacy of the treatment. Cumulative effects can therefore come into play. Moreover, the disposal of heavy-metal-contaminated material is a problem, both at the level of NP production and after (possible) use at the clinical level, posing a threat mainly to aquatic life and soil.[77] Therefore, heavy-metal-free NPs are preferable over classical, Cd- and Pb-based QDs. $(Ag,Cu)In(S,Se,Te)_2$ (even though Ag^+ and $Cu^{+/2+}$ are also cytotoxic),[44,45] InAs, InP, and Ag_2S are possible candidates as far as QDs (or semiconductor nanocrystals more broadly speaking) are concerned. Regarding the other class of candidates for luminescence imaging, RENPs, with a real potential to be used in biomedical applications, are usually based on fluorides or oxides and often contain alkaline metals. Whereas alkaline metal ions can be considered safe, the toxicity of RE^{3+} ions is debated; however, they are generally considered less toxic than heavy metals.[78,79] Toxicity of RE^{3+} is a matter of concern particularly regarding exposure in the workplace *via* inhalation.[78] Nonetheless, further studies have shown that continuous exposure *via* ingestion or injection also has negative effects, including damage to various organs (liver, kidneys, heart, brain; see Table 3 in ref 78 for more details). This negative repercussion is far from unexpected, because RE^{3+} ions are used as catalysts in many reactions, are known to interact with biological molecules,[80] and are thus likely to act as substrate for unwanted reactions within the body.

To prevent metal ion leaching from NPs, a protective shell of inert material can be grown on the surface of both QDs and RENPs, a strategy that usually has the advantage of also increasing the brightness of the luminescent NP. ZnS[89] and CaF_2,[90] both of which do not contain toxic elements, are two exemplary materials for shelling QDs and RENPs, respectively. In addition, Santos *et al.* recently demonstrated how ultrafast laser irradiation can be used to build a protective layer on Ag_2S NPs, ultimately resulting in an increased luminescence bright-

https://dx.doi.org/10.1021/acsnano.0c08349
ACS Nano 2021, 15, 1917–1941

Table 1. Selection of Studies Where Pb-Containing Quantum Dots (QDs) Were Used As Contrast Agents for Fluorescence Imaging[a]

material	λ_{em}^{max} (nm)	PLQY (%)	surface	mouse	injection	conc. (mg/mL)	volume injected (μL)	total mass, mg (mg/kg)[b]	ref
PbS/CdS/ZnS	1270	NA	mercaptopropionic acid	female CD1	r.o./i.v.	0.04	100	0.004 (1.3×10^{-4})	75
PbS/CdS	1650	2.2–22	oleyamine-branched poly(acrylic acid) + PEG	female C57BL/6	i.v.	2	200	0.4 (1.3×10^{-2})	81
PbS	1300	20.3	β-lactoglobulin	female nude	i.v.	0.25	200	0.05 (1.7×10^{-3})	82
PbS:Zn^{2+}	1630	up to 50	oleyamine-branched poly(acrylic acid) + PEG	Balb/C	i.v.	6	100	0.6 (2×10^{-2})	83
PbS	903	NA	silica PEG	male nude	s.c.	1	30	0.03 (1×10^{-3})	84
PbS	900	NA	1,2-diacyl-*sn*-glycero-3-phosphoethanolamine-*N*-[methoxy(poly(ethylene glycol))] (mPEG-DSPE)	Balb/C	i.v.	NA	NA	(2.5×10^{-2})[c]	85
PbS	1308	17.3	RNase	nude	i.v.	26 nM	200	0.001 (3.3×10^{-5})	86
PbS	1050–1220	NA	dihydrolipoic acid–poly(ethylene glycol)	NA	i.v.	0.01	30	0.0003 (1×10^{-5})	87
PbS/CdS/ZnS	1026, 820 (UC)[d]	4.6 (UC)[d]	1,2-diacyl-*sn*-glycero-3-phosphoethanolamine-*N*-[methoxy(poly(ethylene glycol))] (mPEG-DSPE)	Nude	s.c.	3	30	0.09 (3×10^{-3})	88

[a]Reported parameters are from left to right the material composition, maximum of the emission spectrum (λ_{em}^{max}), photoluminescence quantum yield (PLQY), surface chemistry, mouse type, injection modality (r.o. = retroorbital, i.v. = intravenous, s.c. = subcutaneous), concentration of the injected dispersion, total volume injected, and the total injected mass of QDs. PbS QDs were selected as representative of heavy metal-containing nanoparticles (NPs) working in the near-infrared range, where biological tissues are more transparent. [b]In parentheses, we report the mass of NP normalized to the weight of the animal considering a body weight of 30 g for all animals. [c]Value obtained from the toxicity tests rather than from imaging. [d]The produced QDs displayed upconversion (UC) emission.

ness while keeping toxicity to a minimum (Figure 6).[35] Because QDs and RENPs have operation capabilities in both the visible range and the NIR, they are suitable for *in vitro* as well as *in vivo* use. On the other side of the spectrum, carbon-based materials such as CDs and CNTs are the NP of choice when a lack of intrinsic compositional toxicity is a necessity. Moreover, the production of these materials follows green(er) methods, and there is little-to-no issue related to handling of the NP dispersions or the solvents used during their synthesis. However, the emission of CDs is not yet satisfactorily in the BW-I/II range,[91−93] while NIR-emitting CNTs are generally not bright enough and their morphology is a source of worry in terms of toxicological effects (*vide infra*).

> Because quantum dots and rare-earth nanoparticles have operation capabilities in both the visible range and the near-infrared, they are suitable for *in vitro* as well as *in vivo* use.

All this being said, we argue that in the case of a single exposure to inorganic NPs for diagnostic purposes, the drawbacks and risks for the patient associated with the intrinsic toxicity of elements composing the NPs could (in general) be overlooked. However, problems might arise in the study of chronic or slowly developing diseases that would require the acquisition of multiple images (*i.e.*, the repeated administration of inorganic NPs). In this case, the concentration of NPs in organs retaining them could overcome the damage limit. In preclinical units, the use of NPs containing hazardous elements could be justified, particularly for *ex vivo* or *in vitro* experiments aimed at investigating biological phenomena. A gradual farewell, particularly from NPs containing heavy metals, is both far-sighted and judicious. It is foreseeable that restrictions on the use of those hazardous materials might be put into place in the (more or less distant) future. In addition, the toxicological impact of materials containing heavy metals should be considered at different stages of the NP life cycle (production, handling, storage, and disposal). And from this point of view, the risks increase, due to cumulative toxic effects and the possibility of these elements entering the food chain.

> A gradual farewell, particularly from NPs containing heavy metals, is both far-sighted and judicious.

Size and Morphology. One of the important characteristics of NPs is their large surface-to-volume ratio. This geometric consideration is pivotal because it translates to a higher surface available for interaction with the environment. The surface of a material—particularly at the nanoscale, where exceedingly small curvature radii are found—is substantially different from the bulk, featuring vacancies, dangling bonds, and strained lattice.[35,94,95] Thus, overall, the surface of NPs is disseminated with high-energy sites that are highly reactive. Moreover, the surfaces of QDs and RENPs are inherently positively charged due to the presence of exposed metal ions with unsaturated valency.[96] These two last considerations become more relevant when designing surface functionalization strategies. Given the above considerations, it is not surprising that often a trend has

https://dx.doi.org/10.1021/acsnano.0c08349
ACS Nano 2021, 15, 1917−1941

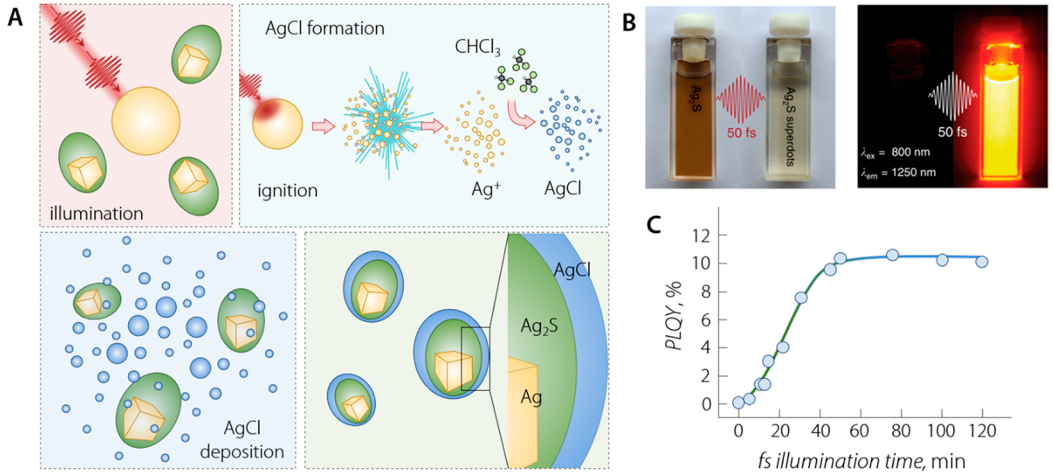

Figure 6. Preparation of Ag_2S/AgCl superdots. (A) The formation of superdots is triggered by irradiation with near-infrared ultrafast laser pulses. This process entails a Coulomb explosion of Ag nanoparticles (NPs) present as byproducts, followed by reaction of the released Ag^+ ions with CH_3Cl to form AgCl, which ultimately deposits on the surface of Ag_2S NPs, forming a protective shell. (B) The emission of the superdots is brighter than that of parent Ag_2S NPs under 800 nm excitation. (C) The increase in photoluminescence quantum yield (PLQY) before and after irradiation is 100-fold. Adapted from ref 35 under the terms of the Creative Commons Attribution License (CC BY 4.0). Copyright 2020 Springer Nature.

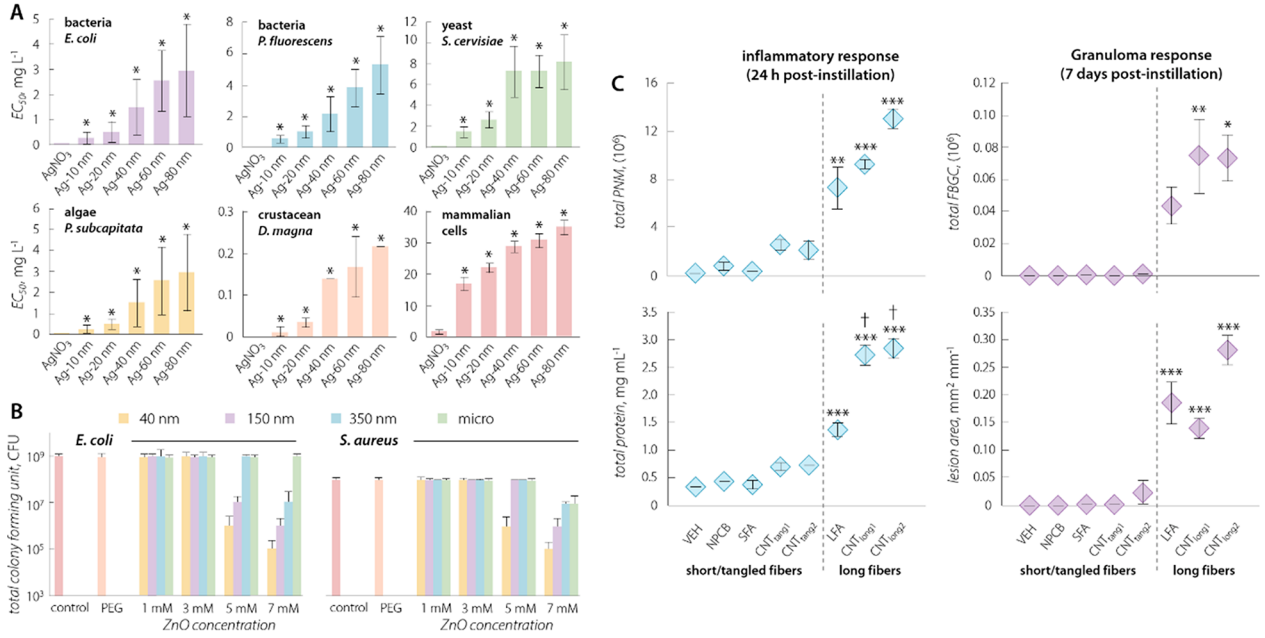

Figure 7. Dependence of toxicity on the size of nanoparticles (NPs). (A) 50% effective concentration (EC_{50}) values obtained after exposing different cellular lines (vegetal and animal) to Ag NPs of different sizes (10, 20, 30, 40, 60, and 80 nm) compared to the effect of a solution of $AgNO_3$. Adapted from ref 97 under the terms of the Creative Commons Attribution License (CC BY 4.0). Copyright 2014 Public Library of Science. (B) ZnO particles show a size- (and concentration-) dependent toxicity toward *E. coli* and *S. aureus*, with smaller NPs more substantially curbing the growth of the respective cell colonies. Reproduced with permission from ref 111. Copyright 2009 Springer Nature. (C) In the case of carbon nanotubes (CNTs), longer fibers elicit a stronger inflammatory response and a larger number of granulomas in the mesothelial lining of the body cavity of mice, compared to shorter or tangled (*i.e.*, effectively smaller and with a smaller aspect ratio) CNTs. Reproduced with permission from ref 112. Copyright 2008 Springer Nature.

been observed correlating smaller NP size with greater toxicity,[97,98] although this is not always the case and case-by-case distinctions should be made (Figure 7).[99]

The size of NPs also affects their penetration capability through specific physical barriers. For example, smaller (20 nm) insulin-coated NPs were found to more efficiently cross the blood–brain barrier (BBB) than larger ones (50 and 70 nm).[100] Similarly, in another study, polysorbate-coated polybutylcyanoacrylate NPs with a size smaller than 100 nm were shown to cross the BBB more effectively.[101] At a cellular level, Guo *et al.* showed that hydrophobic lipid-covered Au NPs feature different kinetics in the translocation through a lipid bilayer.[102] In particular, NPs with a diameter below 5 nm remain trapped in the bilayer, while larger particles can translocate through it. However, as discussed below, the crossing efficiency of NPs into specific tissues and cellular membranes is greatly influenced by the surface chemistry of the NPs, with the probabilities of

https://dx.doi.org/10.1021/acsnano.0c08349
ACS Nano 2021, 15, 1917–1941

accumulating in different brain regions being governed by the type of functionalization.[103,104]

We should observe at this point that NPs in dispersion might form aggregates. Due to geometric factors, these aggregates can interact differently with cells compared to single NPs of equivalent overall volume.[105] Ideally, one would want a dispersion to be administered where single NPs are individually dispersed and do not aggregate over time.[106,107] In this situation, possible enhanced toxicity due to aggregates would be avoided, although there are contrasting reports regarding this potential increased toxicity.[105,106] Preventing the aggregation-induced broadening of the size distribution also reduces the variability in the behavior featured by the NP ensemble (see Figure 3). The colloidal stability and lack of unwanted aggregates in dispersion is, hence, another relevant aspect. To that end, the strategies developed to impart biomimetic/biocompatible features to a NP generally also afford long-term stability to the dispersion. When a NP dispersion is injected intravenously, the flow of the bloodstream is expected to prevent aggregation between the NPs. Thus, aggregation is mainly investigated when the NPs reach a specific tissue. Indeed, sometimes controlled aggregation is harnessed to increase the effectiveness of the delivery at the desired site. For example, pH-[108,109] and microRNA-induced[110] aggregation of Au NPs has been exploited as a means to promote accumulation at solid tumors and retention within cancer cells.

Size is not the only geometric factor at play when gauging the toxicity of NPs. It is a well-established fact now that CNTs, despite their biocompatible chemical composition, have inflammatory and carcinogenic potential on par with the geometrically similar asbestos fibers (Figure 7C).[113] This behavior is a result of the extreme aspect ratio (length/diameter) of CNTs, as also shown by the fact that their toxicity scales with their length (from hundreds of nanometers to a few microns).[112,114] The toxicity of CNTs mainly arises from their inhalation followed by their nesting within the tissues of the lower respiratory tract.[115] As a result, concerns for their use in fluorescence imaging can partially be allayed because dispersions are employed to limit the presence of airborne CNTs. Aside from this specific case, the NPs used in fluorescence imaging are generally much less anisotropic with sphere-like morphologies and low aspect ratios. Therefore, save for CNTs, this aspect is one of the least worrying as far as toxicity is concerned.

Surface Chemistry. This parameter is by far the most important for determining the fate of a NP and its interactions with biological tissues and, thus, both its toxicity and its ability to target specific tissues.[103] The chief impact of surface chemistry over size and morphology has been showcased several times for different NPs (*e.g.*, Au nanorods, RENPs, and QDs).[79,116] For example, heavy-metal-free InP QDs have been shown to exhibit cytotoxicity when featuring amine groups on their surface, whereas hydroxyl- and carboxyl-bearing QDs are not toxic.[117] This cytotoxicity is a direct consequence of the presence of positively charged cationic species ($-NH_3^+$) as compared to negatively charged anionic ones ($-COO^-$). In general, a surface featuring positive charge is associated with higher cytotoxicity, due to its stronger interaction with the cellular membrane.[118] Surface charge is also a key parameter for cellular internalization of NPs, along with size and morphology.[119] The step of internalization is fundamental to guarantee the residence of NPs at the site of interest, and it usually proceeds *via* two types of pathways: endocytosis-based uptake and direct cellular entry. Induced aggregation can also be exploited to avoid exocytosis once the particles have been internalized *via* endocytosis.[110] The pathway by which internalization occurs depends not only on the NP parameters but also on the cell type. For a comprehensive summary of the state-of-the-art of cell uptake and trafficking, the reader is encouraged to read the recent review by Donahue *et al.*[119]

> Surface chemistry is by far the most important parameter for determining the fate of a nanoparticle and its interactions with biological tissues and, thus, both its toxicity and its ability to target specific tissues.

The subject of surface functionalization of NPs is incredibly broad, and its discussion is a consistent element in many review articles dedicated to the use of NPs for biomedical applications.[119−123] Simply put, a successful surface functionalization boils down to finding the right balance between minimizing interactions with biological components that elicit an immune response (and, hence, premature clearance of the NPs), while prompting selective recognition of and interaction with cells that form the tissue of interest. Silica coating[124−126] as well as the use of zwitterionic molecules[127,128] or polymers[129] are among the most explored strategies to enhance biocompatibility and extend NP circulation time. Decoration with polyethylene glycol (PEG), in particular, is often regarded as the golden standard for imparting "stealth" properties to NPs.[130,131] This approach builds on the success obtained with PEGylation of proteins in terms of improving circulation time by preventing uptake from macrophages.[132] However, studies have shown that PEG antibodies are produced upon repeated injections of PEGylated species.[133,134] In terms of fluorescence imaging, this finding translates to a possible premature uptake of the PEGylated contrast agent, leading to a shorter circulation time and less effective accumulation at the desired site.

> A successful surface functionalization boils down to finding the right balance between minimizing interactions with biological components that elicit an immune response (and hence premature clearance of the nanoparticles), while prompting selective recognition of and interaction with cells that form the tissue of interest.

But, even considering perfectly stealthy NPs, how do we achieve their selective accumulation at the desired site? The literature contains countless examples of intratumoral injection of NP dispersions followed by imaging and/or treatment of the tumor.[135−137] However, these approaches have limited appeal in clinical practice, and they are justified in proof-of-concept studies, where emphasis is put on the side of the material or an innovative treatment. The ideal strategy entails the engineering of a NP so that it can be injected intravenously in the proximity of the tissue of concern and then autonomously identifies and accumulates in correspondence with the targeted cells.[138] This scenario can be achived by taking advantage of two approaches:

https://dx.doi.org/10.1021/acsnano.0c08349
ACS Nano 2021, 15, 1917−1941

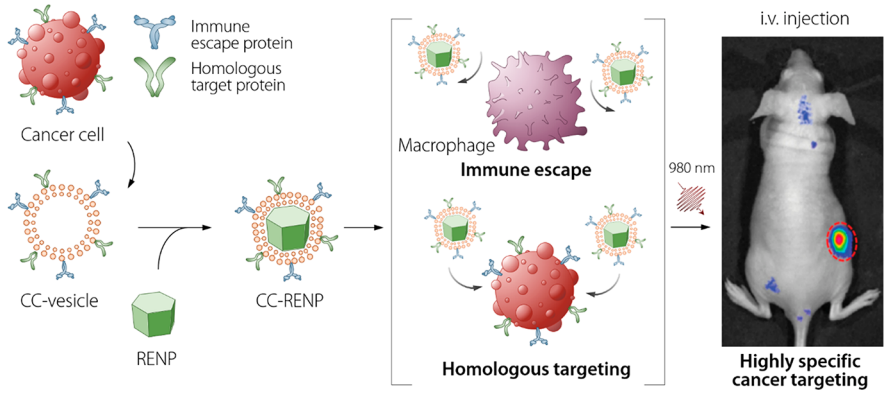

Figure 8. Scheme of the preparation, action, and use of the rare-earth-nanoparticle (RENP) coated with a cancer cell vesicle. The membrane of cancer cells can be used to prepare vesicle bearing membrane proteins. RENPs (in this case, $NaYF_4$:Yb^{3+},Er^{3+}) can be encapsulated in this vesicle. The resulting vesicle-coated RENP exhibits immune escaping and homologous targeting capabilities inherited from the source cancer cells. Adapted with permission from ref 147. Copyright 2016 John Wiley and Sons.

passive and active targeting.[139,140] Passive targeting is applicable when targeting solid tumors because it leverages the enhanced permeation and retention (EPR) effect: The natural extravasation of NPs to tumoral tissues where the blood vessels are defective (fenestrated). However, better selectivity is achieved by tethering targeting moieties to the surface of the NP. Folic acid, small peptides, antibodies, aptamers, and other biologically active molecules have all been used to target specific cells.[141,142] The complementarity between the moieties attached to the NPs and cellular receptors is critical to successful accumulation and cellular internalization. In some cases, physical barriers must be overcome to reach a particular tissue. The most famous and difficult barrier to cross is arguably the BBB, whose effectiveness in preventing nonspecific crossing (and, thus, in protecting our brain) is also the reason for the difficulty in accessing the brain with NPs through the circulatory system.[143] However, the brain is not the only organ/tissue that is difficult to reach. A great deal of effort is being invested in improving the targeting efficiency of tumors after intravenous injection of NPs.[144] Despite this trend, the current targeting efficiency (percentage of injected NPs reaching tumor site) has been reported to be below 1%. Therefore, future investigations devoted to modifying the pharmacokinetics of injected NPs to increase the targeting efficiency are desirable.

We believe that significant future research efforts for NP surface functionalization should be directed toward the personalization of nanomedicine.[145] One powerful approach is to use the cell membranes already present in the body,[146] thus relying on the naturally available products of millions of years of cellular evolution. For example, researchers have shown that by using xenografts from patients, one can prepare cancer-cell-membrane-coated NPs for personalized cancer treatment or tumor imaging (Figure 8).[147,148] This approach exploits the tendency of tumor cells to adhere one to another, which can be harnessed to promote accumulation of coated NPs at the tumor site. Red blood cells and platelets can be used as sources of biomimetic membranes, as well,[149,150] because they are recognized as endogenous components from the body, thus eliminating risks of NP opsonization and premature clearance.

Further functionalization (either *via* surface conjugation or lipid insertion) can be performed to enhance selective targeting capabilities. Any cell membrane can be used depending on the foreseen use of the NPs. This approach might also avoid or limit the formation of a so-called protein corona (PC) atop the NPs

We believe that future research efforts for nanoparticle surface functionalization should be directed toward the personalization of nanomedicine.

when they enter a bodily fluid (Figure 9).[151] This PC is composed of proteins found in the body fluid, and its

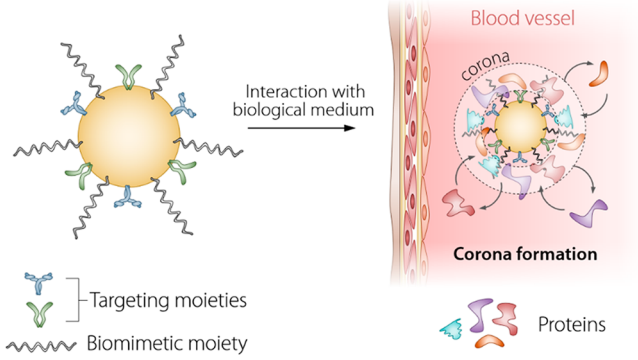

Figure 9. Protein corona (PC) formation. When a nanoparticle (NP) enters the body and comes into contact with a biological fluid, the proteins that are present in the fluid interact with the surface of the exogenous species. Different proteins have different affinities toward the surface of the NP. This differential affinity results in a composition of the PC that depends on the surface chemistry of the NP as well as the nature of the bodily fluid. Note that due to the adsorption of these proteins, the bioactive form of the NP (*i.e.*, bearing a PC) is *de facto* a different species from the one before the injection in the body, to the point of potentially compromising the targeting capabilities of the NP.

composition determines the fate of the NP, governing the interaction with biological species.[152] Indeed, even PEGylated nanoformulations approved for medical use become covered by the PC, which has the fingerprint of the environment in which the NPs are introduced.[153] The use of cell membranes that are already present in the body to coat the NPs should minimize issues related with PC formation and changes in the NP surface chemistry induced by it. Customization of nanoformulations by encapsulation of NPs within the membranes of cells extracted from the patient and their further functionalization with

https://dx.doi.org/10.1021/acsnano.0c08349
ACS Nano 2021, 15, 1917−1941

(bio)molecules to enhance active targeting is expected to open the door to ever more effective diagnosis and treatment of a number of diseases. As we discuss in the next section, for the specific case of luminescence imaging, these opportunities are restricted by some physical considerations that are intrinsic of the imaging modality.

Brightness and Tissue-Induced Attenuation: Will We Ever Give It the Required Attention? In NP-based fluorescence imaging, the signal level is of paramount importance. An ever-increasing number of technologies aimed at improving the contrast between the signal level and the autofluorescence present in biological tissues have been proposed of late. Perhaps the most remarkable technology entails the incorporation of time-dependent analysis of fluorescence images obtained under excitation with a pulsed source.[154−156] This strategy affords the removal of the background contribution of autofluorescence (characteristic of biological tissues) and significantly improves the quality of the image. Nevertheless, even after applying this general optimization procedure, some drawbacks remain difficult to circumvent under *in vivo* conditions, namely tissue-induced attenuation of light and the low fluorescence efficiency of NPs. Thus, to expand the applicability of NP-based fluorescence imaging, a two-pronged approach is necessary: (i) increase the fluorescent efficiency (fluorescence brightness, defined below) and (ii) minimize the effects of the optical extinction caused by tissues.

Looking for Brighter Nanoparticles. The pursuit of evermore bright NPs is an ongoing process. In fluorescence imaging, one of the main drivers for this search is the fact that if brighter NPs are used, fewer of them are required for acquiring an image. The ability to use fewer NPs alleviates concerns related to the injection of a large number of exogenous species in the body and the possible adverse effects they might have. One of the most important parameters for improving the fluorescence of a given NP is the PLQY.[157] PLQY (Φ) is defined as the ratio between the number of photons emitted and the number of photons absorbed.[158] Although researchers looking for high-brightness NPs often focus on increasing the PLQY, years of experience have shown that this strategy is insufficient, as a high PLQY coupled with low absorption efficiency of the excitation light also yields a poorly luminescent material. To account for the interplay between these two quantities, the concept of brightness (PLQY times the absorption coefficient) is introduced, which is especially useful when comparing different luminescent materials or probes.[158]

Two strategies can be used simultaneously to increase the NP brightness: the development of highly absorptive NPs and the modification of the NP structure to enhance the PLQY. The second half of this two-pronged approach implies the enhancement of radiative transition probabilities. In NPs, this enhancement is achieved by reducing surface defects that act as luminescence quenchers and isolating the NP from environmental molecules whose vibrations promote nonradiative decays.[159,160] The preparation of core/shell structures is an optimal approach in this context. The presence of a protective shell has been widely demonstrated to produce significant enhancements in the PLQY of luminescent NPs.[74,161] Unfortunately, one-size-fits-all solutions do not exist. One example of this issue is PbS QDs, whose PLQY cannot be effectively increased *via* ZnS shelling,[162] even though this strategy has proven successful with most semiconductor NPs.[89,163] Some of the authors of this Perspective recently demonstrated how combining ultrafast photochemistry with traditional wet chemistry could lead to core/shell Ag_2S NPs with PLQY close to 10% (as illustrated in Figure 6).[35] This is a remarkable result, considering the usually low values of PLQY featured by Ag_2S NPs.[164] Following this path, we believe that more unconventional yet effective strategies might and should be developed to push the boundaries of achievable PLQY.

One can also focus on increasing the excitation light absorption capability of the NP. In this context, QDs have an edge on RENPs, with a light absorption cross-section that is 3−10 orders of magnitude larger ($\sigma_{QD} = 10^{-17}-10^{-11}$ cm^2 *vs* $\sigma_{RE} = 10^{-21}-10^{-20}$ cm^2). CNTs also have a larger absorption cross-section compared to single RE^{3+} ions ($\sigma_{CNT} = 10^{-18}-10^{-17}$ cm^2). No reliable data could be found for single-photon excitation of CDs; multiple-photon excitation processes are instead much better quantified in these NPs.[165] Given the poor absorption capabilities of RE^{3+} (owing to the forbidden 4f−4f nature of most of the electronic transitions involved in the photoluminescence of these ions),[166] RENPs are contrast agents that would substantially benefit from a boost of their light-harvesting prowess.[167,168] To that end, researchers have coupled semiconductor NPs and RE^{3+} both decorating RENPs with Ag_2S[169] or Ag_2Se[170] NPs and doping RE^{3+} ions in QDs.[171] These strategies are incredibly advantageous on paper, but their efficiency strongly depends on (and is often limited by) how effectively the energy is transferred from the absorbing moiety (semiconductor NP) to the emitting RE^{3+} ion. This consideration is equally relevant when organic dyes (antennas) are employed as light harvesting species for the enhancement of RE^{3+} brightness.[168] The use of plasmonic moieties coupled to luminescent NPs is another highly coveted strategy, which has been used on several occasions to enhance the absorption and/or emission efficiency of RENPs[172] and QDs.[173] Harnessing the plasmonic effect is also challenging because quenching can be prompted, rather than photoluminescence enhancement, if the relative position between plasmonic moiety and fluorescent NP is not precisely controlled.[174]

All in all, we believe that a combination of strategies to increase PLQY (*e.g.*, *ad hoc* developed shelling procedure) and absorption (*e.g.*, plasmon-induced improvement of absorption and/or emission probability) would lead to brighter contrast agents whose use could improve the performance of fluorescence imaging.

> A combination of strategies to increase photoluminescence quantum yield and absorption could lead to brighter contrast agents whose use would improve the performance of fluorescence imaging.

Tissue Attenuation. Even with the brightest possible NP as the contrast agent, the problem of low-contrast images still poses a serious impediment. Further limitations need to be considered, some of which could be overcome and others would have to be embraced by the scientific community. The latter is the case, for example, of the conditions imposed on the irradiation dose.[175−178] The issue of light attenuation in a biological system is difficult to tackle, as it is entirely determined by the optical properties of the tissues (Figure 10).[179−181] Although the exploitation of BWs in the electromagnetic spectrum minimizes these problems,[11,182,183] the strategy does not completely

https://dx.doi.org/10.1021/acsnano.0c08349
ACS Nano 2021, 15, 1917−1941

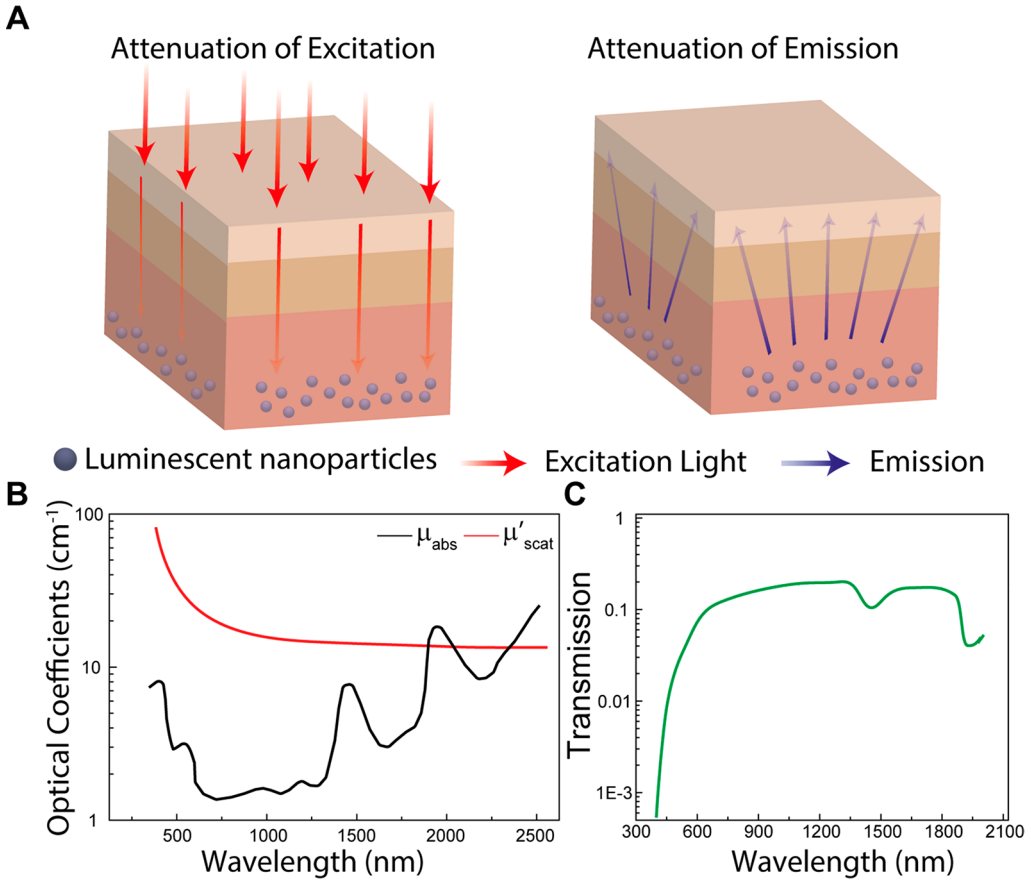

Figure 10. Effects of light attenuation in biological tissues. (A) Simplified depiction of the transmission of excitation (left) and emission (right) through biological tissues. (B) Wavelength dependence of the absorption and reduced scattering coefficients of human skin in the visible and near-infrared ranges.[186] (C) Percentage of light that successfully passes through 1 mm of human skin as a function of the wavelength.

resolve them. For the sake of illustrating the implications of these restrictions, let us consider an idealized luminescent NP with a quantum energy efficiency (defined as the ratio between the energy output and the energy input)[158] of 100%. Even in the situation where this material is found underneath a layer of one of the most transparent human tissues in the BWs (gray matter, for example),[184] both the excitation and emission light are still absorbed and scattered. For our purposes, let us also consider the use of a BW-I excitation source, as it has been shown to minimize undesired heating effects,[30,31,185] and that the emission falls within BW-II. Considering that the more external part of the gray matter has a usual thickness of 10 mm and average attenuation coefficients of 0.07 mm^{-1} and 0.06 mm^{-1} in BW-I and BW-II, respectively, this means that 50% of the excitation light does not reach the NP and that 45% of the subsequently generated emission is not transmitted to the detection system. Compared to the case in which the sample is directly illuminated by the laser, in this example 73% of the intended emission is lost. Such a value might still be acceptable for biomedical applications. However, had another tissue been chosen, the total loss would be even higher. The skin, for example, has average attenuation coefficients of 16.0 mm^{-1} and 16.6 mm^{-1} in BW-I and BW-II and would provide a total loss of more than 90%.[18,186] The situation is worsened by real-life scenarios where several tissues with different optical properties are simultaneously affecting photon propagation. In addition, NPs used as contrast agents have quantum energy efficiencies below 100%.

Pathways to Address the "Tissue Attenuation" Issue. To alleviate the negative repercussions of these large attenuations, one could try either of these two solutions: (i) increase the excitation power so that more excitation photons reach the contrast agent, causing more photons to be emitted and, therefore, detected or (ii) increase the exposure time so that more signal is collected. Although the first approach may prove useful in fields such as fluidics and electronics, it is not viable when dealing with biological tissues. Because certain safety guidelines need to be followed, the irradiation dose must never surpass a well-established maximum value.[175−178] Though there are minor disagreements in the literature, a maximum excitation power density of 330 mW/cm^2 is generally accepted for the study of tissues under normal conditions.[175,187] If a photothermal treatment is being induced, however, this maximum value could reach up to 2 W/cm^2.[188] Be that as it may, increasing the excitation power is neither a safe nor a universal approach. Contrastingly, increasing the exposure time does not necessarily compromise the health status of the tissue if the irradiation dose is within the safety limits. Increased exposure time generates other problems, however, including loss in temporal resolution and accumulative heating during illumination. Furthermore, the effectiveness of the approach might also be compromised by the technological limits of the detection systems. For example, even after increasing the exposure time, if the transmitted intensity is only slightly larger than the noise-equivalent irradiance (NEI; *i.e.*, the flux density that results in a signal-to-noise ratio of 1) of

https://dx.doi.org/10.1021/acsnano.0c08349
ACS Nano 2021, 15, 1917−1941

Table 2. Potential of luminescent Nanoparticles for Noninvasive Applications in Human Tissues[a]

Tissue	$\langle\mu'_{scat}\rangle$ (cm^{-1})	$\langle\mu_{abs}\rangle$ (cm^{-1})	Surrounding Tissues	I_{det}/I_{emi} (%)	I_{exc}^{del}/I_{exc} (%)	κ_{det}^{max} (W/cm^2)
Skin[17, 185] (1.5 mm)	BW-I: 15.6 BW-II: 16.3	BW-I: 0.38 BW-II: 0.34	--	8.2	9.0	2.4×10^{-3}
Adipose tissue[185] (7 mm)	BW-I: 11.2 BW-II: 8.68	BW-I: 1.08 BW-II: 1.00	Skin (1.5 mm)	2.8×10^{-3}	1.3×10^{-3}	1.2×10^{-10}
Muscles[185] (10–30 mm)	BW-I: 5.95 BW-II: 5.73	BW-I: 0.46 BW-II: 0.51	Skin (1.5 mm), adipose tissue (7 mm)	$8.1\times10^{-7} - 8.3\times10^{-4}$	$1.1\times10^{-7} - 8.8\times10^{-4}$	$2.9\times10^{-18} - 2.4\times10^{-11}$
Skull[215] (6 mm)	BW-I: 20 BW-II: 16	BW-I: 0.1 BW-II: 0.5	Skin (1.5 mm), possibly facial muscles (15 mm)	$5.0\times10^{-6} - 6.0\times10^{-2}$	$1.5\times10^{-6} - 2.2\times10^{-2}$	$2.4\times10^{-16} - 4.3\times10^{-8}$
Chest wall[216] (14 mm)	BW-I: 46.1 BW-II: --	BW-I: 1.29 BW-II: --	Skin (1.5 mm), adipose tissue (7 mm)	6.3×10^{-12}	6.6×10^{-18}	1.37×10^{-33}
Bone[16, 217, 218] (up to 25 mm)	BW-I: 16 BW-II: 10.5	BW-I: 0.02 BW-II: 0.07	Skin (1.5 mm), adipose tissue (7 mm), possibly muscle (up to 30 mm)	$3.1\times10^{-14} - 1.3\times10^{-1}$	$6.8\times10^{-21} - 2.2\times10^{-2}$	$6.9\times10^{-39} - 9.4\times10^{-8}$
Dura mater[219] (2.5 mm)	BW-I: 8.27 BW-II: 9.52	BW-I: 0.5 BW-II: --	Skin (1.5 mm), Skull (6 mm)	1.8×10^{-5}	1.2×10^{-4}	7.2×10^{-14}
Breast[220] (up to 55 mm)	BW-I: 12.0 BW-II: 10.0	BW-I: 0.13 BW-II: 0.20	Skin (1.5 mm), adipose tissue (7 mm)	$2.1\times10^{-9} - 3.5\times10^{-7}$	$2.1\times10^{-11} - 9.0\times10^{-7}$	$1.4\times10^{-24} - 1.0\times10^{-17}$
Parietal peritoneum[221] (14 mm)	BW-I: 11.0 BW-II: 11.0	BW-I: 12.0 BW-II: 10.0	Skin (1.5 mm), adipose tissue (7 mm), muscle (5.6 mm)	6.7×10^{-5}	1.8×10^{-5}	4.0×10^{-14}
Stomach[222] (46 mm)	BW-I: 7.59 BW-II: 7.62	BW-I: 1.0 BW-II: 2.5	Skin (1.5 mm), adipose tissue (15 mm), muscle (5.6 cm), parietal peritoneum (1.4 mm)	$9.6\times10^{-18} - 2.9\times10^{-12}$	$6.6\times10^{-18} - 1.5\times10^{-13}$	$2.1\times10^{-39} - 1.4\times10^{-29}$
Liver[223] (69.6 mm)	BW-I: 9.0 BW-II: 7.68	BW-I: 1.0 BW-II: 0.5	Skin (1.5 mm), adipose tissue (15 mm), muscle (5.6 mm), parietal peritoneum (1.4 mm)	$4.6\times10^{-20} - 2.7\times10^{-14}$	$1.6\times10^{-24} - 4.5\times10^{-17}$	$2.4\times10^{-48} - 4.0\times10^{-35}$
Lung[224] (102 mm)	BW-I: 20 BW-II: --	BW-I: 0.01 BW-II: --	Skin (1.5 mm), adipose tissue (7 mm), chest wall (14 mm)	$2.4\times10^{-54} - 7.9\times10^{-16}$	$9.1\times10^{-76} - 7.0\times10^{-21}$	$7.2\times10^{-134} - 1.8\times10^{-40}$
Intestine[219] (73.3 mm)	BW-I: 9.66 BW-II: 8.56	BW-I: 1.5 BW-II: 2.3	Skin (1.5 mm), adipose tissue (15 mm), muscle (3 mm), parietal peritoneum (1.4 mm)	$9.9\times10^{-11} - 6.5\times10^{-9}$	$1.1\times10^{-11} - 9.9\times10^{-11}$	$3.6\times10^{-26} - 2.1\times10^{-23}$
Brain (grey matter)[183] (10 mm)	BW-I: 0.7 BW-II: 0.6	BW-I: 0.02 BW-II: 0.04	Skin (15 mm), skull (6 mm), dura Mater (2.5 mm)	$2.6\times10^{-5} - 3.6\times10^{-5}$	$4.1\times10^{-6} - 5.8\times10^{-6}$	$3.5\times10^{-15} - 6.9\times10^{-15}$
Brain (white matter)[183] (15 mm)	BW-I: 5.2 BW-II: 3.0	BW-I: 0.08 BW-II: 1.00	Skin (15 mm), skull (6 mm), dura mater (2.5 mm), grey matter (up to 29 mm)	$1.8\times10^{-7} - 3.7\times10^{-7}$	$1.4\times10^{-8} - 5.5\times10^{-8}$	$8.3\times10^{-20} - 6.7\times10^{-19}$
Maxillary sinus[219] (15 mm)	BW-I: 6.07 BW-II: 4.79	BW-I: 1.00 BW-II: 1.00	skin (15 mm), skull (6 mm)	$5.4\times10^{-6} - 7.2\times10^{-5}$	$3.7\times10^{-7} - 6.3\times10^{-6}$	$6.6\times10^{-17} - 1.5\times10^{-14}$

[a]Estimation of the emitted light that is detected (column 4), the excitation light that reaches the inner part of the tissue (column 5), the detected power density after considering an excitation irradiance of 330 mW/cm^2 and luminescent nanoparticles (NPs) with perfect quantum energy efficiency (column 6). In the more internal organs, the NPs were considered to be located between the center of the organ and the proximities of its surface. The rightmost column contains the values of maximum detected irradiance and classifies the different organs according to the possibility of detecting the emission coming from nanoparticles found within them. Four categories are found: optimal (green), circumstantially positive (blue), potentially positive (orange), and negative (red). Dimensions were estimated with cryosections of the human body as provided by *The Visible Human Project*.[214,215]

the camera, the detected signal will be too poor for an accurate analysis.

Because these problems are mainly imposed by the optical properties of the various biological tissues, their corresponding

https://dx.doi.org/10.1021/acsnano.0c08349
ACS Nano 2021, 15, 1917–1941

solutions can only be resolved if one tries first to determine the best possible outcomes when dealing with different organs. Only then can expectations become realistic. To illustrate this concept, we evaluated the potential of narrowband NIR-emitting NPs for applications in various human organs. For the sake of brevity, we chose a model NP that can be excited in BW-I and that emits in BW-II, which is a common situation.[27,189−191] For each case studied, the NPs were considered to have preferential accumulation in a specific organ. The optical properties of this organ, in turn, were registered (according to literature) alongside those of the surrounding tissues. By taking into account their average thicknesses in an adult, it was possible to determine, in a first approximation, (i) the fraction of excitation light that gets into the organ I_{exc}^{del}/I_{exc} and (ii) the fraction of emitted light that gets detected, I_{det}/I_{em}. The main results are included in Table 2 and reveal that, granted that luminescent NPs could accumulate in any desired human organ, most resulting measurements would still be problematic. Many organs provide values of I_{det}/I_{em} and I_{exc}^{del}/I_{exc} below 10^{-8}%. Thus, depending on the excitation energy initially delivered, the emitted light might not be detected at all. To verify which cases could result in viable applications, we considered, without loss of generality, the excitation irradiance to be $\kappa_{exc} = 330$ mW/cm^2 (*i.e.*, the allowed maximum).[175] Under such conditions, the maximum detected irradiance, k_{det}^{max}, is obtained through:

$$\kappa_{det}^{max} = \kappa_{exc}\left(\frac{I_{exc}^{del}}{I_{exc}}\right)\eta\left(\frac{I_{det}}{I_{em}}\right) \quad (1)$$

where η is the quantum energy efficiency of the NPs. If we, once again, consider the best-case scenario where η is equal to 100% (maximum imposed by energy conservation), we then find the data included in the rightmost column of Table 2. By taking into account that the noise-equivalent irradiance (at 1 s of exposure time) of InGaAs cameras currently available in the market is on the order of 10^{-12} W/cm^2,[192] then the straightforward conclusion is that NP luminescence could only be detected in a small set of human organs. Broadly speaking, Table 2 presents at least four different situations:

- Optimal: k_{det}^{max} always exceeds the order of 10^{-12} W/cm^2. The organs that satisfy this condition are highlighted in green in the last column. If luminescent NPs are located within these organs, their light is very likely to be detected.
- Circumstantially positive: k_{det}^{max} is circumstantially higher than 10^{-12} W/cm^2 (highlighted in blue). This is the case, for example, of bones. Depending on which bone is selected, there might be ample muscle tissue around it and, consequently, more attenuation. Other bones (such as those in the hands and feet) might be less affected by attenuation.
- Potentially positive: k_{det}^{max} between 10^{-18} W/cm^2 and 10^{-12} W/cm^2 (*i.e.*, lower than NEI but only by a few orders of magnitude). Although below the detection limits, the possibility of detecting light coming from these organs could have been negatively affected by the first-order nature of the approximation. This issue is important to consider because a simple Beer−Lambert law analysis cannot account for the role of the geometry of the tissue and, for example, the non-additivity of the scattering effect. Furthermore, there is no consensus on their optical coefficients (differences of up to 40% in the mean value have been reported in different works in the literature).[193−199] These facts, together with the possibility of increasing the exposure time or the excitation irradiance (photothermal therapy), could actually result in light being detected. Therefore, by recognizing the limits of our approximations and the accuracy of the data provided in literature, we were led to classify these as potential candidates to be imaged *via* NP-enabled fluorescence imaging. They are highlighted in orange.
- Negative: Organs that had a k_{det}^{max} below 10^{-18} W/cm^2. For these organs, the application of luminescent NPs is not viable even after considering the discrepancies in literature over their optical properties and the simplified nature of the approximations. To justify such a value, one only needs to think about the worst-case scenario where (i) the Beer−Lambert Law, (ii) the discrepancy on the optical coefficients, and (iii) the low integration time (or low excitation irradiance) is each reducing the value of k_{det}^{max} by 2 orders of magnitude. If that were the case, k_{det}^{max} would still fall behind 10^{-12} W/cm^2. Such organs are highlighted in red.

Careful examination of Table 2 suggests that, with the optical coefficients currently reported, luminescent NPs and fluorescence imaging can only be feasibly applied in five main human tissues: skin, bone, muscle, breast, and the outer part of the brain (Figure 11). This conclusion is certainly more modest than what most reports on *in vivo* applications of luminescent NPs in animal models may suggest. The reason why these studies tend to overestimate the potential for human applications is primarily related to the reduced dimensions of the animal under investigation. If one inserts NPs into the livers of mice, an organ which for humans is outside the detection range, the maximum detected irradiance is on the order of 10^{-4} W/cm^2 (assuming similar values for the attenuation coefficients and the dimensions of tissues provided in literature[200−202]) under 330 mW/cm^2 excitation. Such a value is far above the lower detection limit of currently available cameras. The community needs to be careful not to extrapolate their goals from animal models to humans when interpreting research results.

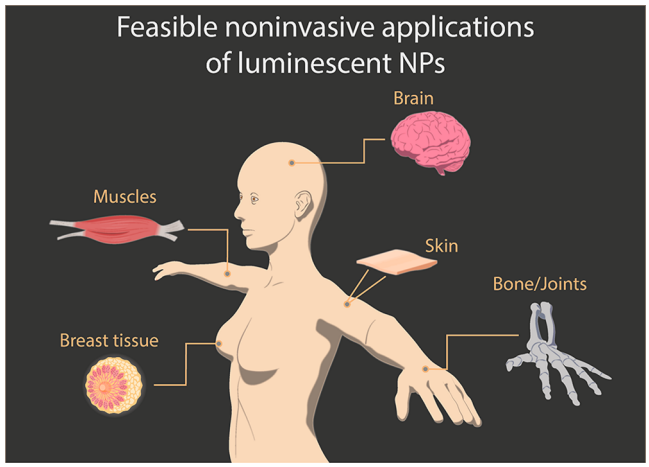

Figure 11. Feasible noninvasive applications of fluorescence imaging through luminescent nanoparticles (NPs). Main human tissues identified as optimal (or at least possible) for investigation with NP-based fluorescence imaging after considering the limitations imposed by the scattering and absorption of near-infrared light in biological tissues. The identification was based on the data inserted in Table 2.

https://dx.doi.org/10.1021/acsnano.0c08349
ACS Nano 2021, 15, 1917−1941

The community needs to be careful not to extrapolate their goals from animal models to humans when interpreting research results.

Nevertheless, even if expectations are lowered, we should not disregard the effort put into luminescence-based nanotechnology in the past decades. Luminescent NPs can still play a role in the noninvasive detection and treatment of several malfunctions of the human body, including diseases such as osteoporosis, vitiligo, multiple sclerosis, stroke, breast cancer, and many others. Furthermore, the already established applications at the small-animal level are also beneficial for better understanding the biological processes that take place during malfunctions of the body. The future of the field, therefore, remains promising. Interestingly, the five human tissues that were selected for Figure 11 form the same set of tissues that have been successfully studied in a well-established technique known as diffuse optical tomography (DOT).[203−212] DOT is an ongoing imaging modality in which a tissue is illuminated by NIR light from an array of sources. Under such conditions, the scattered light that emerges from the tissue is observed with an array of detectors, and then a model of light propagation is used to infer the optical properties of the illuminated tissue. Fluorescence imaging and DOT have similar applicability in that they are both limited by the level of tissue-induced attenuation. Researchers should be attentive to a overlaps between the two techniques as well as their relative advantages, disadvantages, and possible synergies.

Albeit the noninvasive use of luminescent NPs in adult humans is limited to specific tissues, we are more optimistic for uses involving infants and children. Due to the reduced dimensions of their tissues, the number of organs considered viable as indicated in Table 2 would increase, potentially giving rise to more possibilities for the detection and treatment of diseases. Such a concept, in fact, has already been explored in DOT for deep-brain studies in newborn babies.[204,213] Considering all the extra quality checks that will need to be fulfilled for use in newborns, if luminescence-based nanotechnology follows a similar path, then the development of the materials should start focusing on these quality checks at the level of material design. If, however, the intention is still to keep the applicability of luminescent NPs as broad as possible (including adults), then the use of endoscopic techniques will have to be considered. If an endoscope is placed in the proximity of the tissue of interest, the light coming from there can still be collected. Under this circumstance, however, noninvasiveness could no longer be considered as one of the most attractive features of luminescent NPs.

Raising the Stakes: Fluorescence Imaging and Machine Learning. After laying out the problems related to the intrinsic limitations of fluorescence imaging imposed by the properties of luminescent NPs, tissue properties, and measurement setups, let us now delve into how AI can provide a helping hand in this framework.

If we consider the use of fluorescence imaging in preclinical units, in addition to the problem of strong tissue-induced attenuation described in the previous section, the acquisition of fluorescence images requires complete immobilization of the animal under study. Typical integration times used for the acquisition of high-contrast *in vivo* fluorescence images are in the 0.1−1 s range. During this acquisition time, the displacement of a free mouse could be as large as 1 cm. This displacement causes blurring in the acquired image. Traditionally, this challenge has been solved by immobilizing the animal under study, usually by administering anesthesia. This approach not only avoids

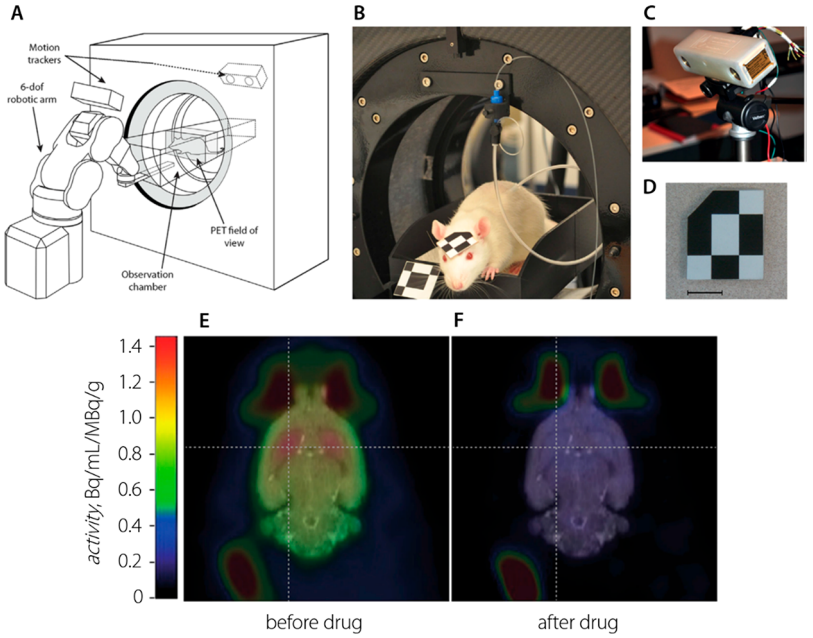

Figure 12. Acquisition of positron emission tomography (PET) images in awake animal models. (A) System designed by Kyme *et al.* for the acquisition of PET images of (B) a moving animal located in an enclosure (C) whose motion is tracked with the use of a pair of CCD cameras that can detect the accurate position of three rigid markers (D), one of which is attached to the head of the animal and the other two at fixed positions. Motion-corrected PET images of the brain were obtained (E) 20 min before and (F) 20 min after drug (amphetamine) administration by following the displacement of [^{11}C]raclopride by unlabeled raclopride.[230] The PET images in (E) and (F) are superimposed on MRI images. Reprinted with permission from ref 230. Copyright 2019 Elsevier.

https://dx.doi.org/10.1021/acsnano.0c08349
ACS Nano 2021, 15, 1917−1941

blurring, it also enables the use of longer integration times, thus improving the signal-to-background ratio in the fluorescence images. However, depending on the goal of the imaging procedure, using anesthesia or physical constraints can be far from ideal. Anesthesia is known to alter vital functions,[226,227] and several works have reported a general decrease of metabolic activity and whole-body temperature during anesthesia procedures. Thus, readouts regarding vital parameters extracted from the analysis of fluorescence images taken on an anesthetized animal could be misleading or erroneous, because the system under investigation is altered by the measurement procedure. This factor could be especially relevant when imaging organs that are more heavily affected by anesthesia, such as the brain.[227−229] To overcome this limitation, imaging of freely moving animals becomes imperative. Indeed, this need has motivated the community to upgrade traditional techniques. For example, Kyme and co-workers developed an experimental setup capable of acquiring PET images in "freely" moving, awake rats.[230] The experimental system (Figure 12) consisted of an unmodified small animal PET system, a robot-controlled animal enclosure, and an optical motion-tracking device.[230]

Using this system, the authors were able to image the impact of drug (amphetamine) administration on brain activity without the need for immobilization. However, the system still imposed severe motion restrictions to the animal owing to the reduced space. Space restrictions limit the potential of this approach to one-animal studies and puts an end to the possibility of studying the impact that social interactions have on vital function. Nonetheless, this study demonstrates that the community is becoming aware of the importance of moving away from anesthesia to obtain results that paint a more truthful picture. The acquisition of fluorescence images of freely moving animals is a challenging task. Because of the use of excitation laser sources and fluorescence cameras, two main technical limitations need to be overcome. First, the technology required to localize the animal within the experimentation cage should be incorporated into the imaging system. Second, a new procedure for imaging acquisition and analysis to correct blurring caused by the rapid movements of the animal becomes essential. This latter point requires knowledge of the animal's position as well as prediction of its motion. These two requirements can be satisfied simultaneously by using AI. To that end, deep learning has been recently applied for real-time tracking and motion prediction of freely moving animals.[231]

We anticipate that, in the near future, these algorithms could be implemented in fluorescence imaging systems already working in preclinical units. Knowing the exact location of the animal is necessary not only for determining the imaging field-of-view but also for selective and accurate excitation of contrast agents within the animal. This goal could be accomplished with the use of advanced optomechanics, which, guided by the output of deep-learning algorithms, could direct the excitation light inside the experimentation cage with high spatiotemporal precision. In this scheme, AI could also be used to develop a module capable of combining information about animal position and motion together with the acquired fluorescence images to correct for image blurring. We foresee that the implementation of AI-based technologies in this field could take time, but we are convinced that the future of fluorescence imaging in preclinical units will be experimentation of freely moving animals.

Lastly, a point must be made regarding spatial resolution, which is relevant both in preclinical and in foreseeable clinical applications. As noted in Table 2, spatial resolution is primarily dependent on the scattering of the light emitted by the contrast agent at a specific depth within the tissue. Due to difference in optical properties, not all the tissues would afford the same spatial resolution in fluorescence imaging. To mitigate this issue, the use of AI could prove advantageous because it is efficient not only in image processing but also in the solution of partial differential equation-related problems (such as the propagation of light).[232] Indeed, convolutional neural networks have been successfully applied in CT,[233−235] MRI,[236−238] and, more recently, in DOT.[239,240] With regards to fluorescence imaging, this technique could train neural networks to reverse the problem of nonlinear photon scattering and, as a consequence, reconstruct the original fluorescence signal coming from the NPs before being transmitted through the different sets of tissues.[239] Such an application could extend the applicability of the field and even offer information on the possible anomalies present in organs and tissues.

PERSPECTIVE AND OUTLOOK

The fate of NP-enabled *in vivo* fluorescence imaging is contingent upon how specific features of luminescent NPs are upgraded in the immediate future. We identify three lines of action:

- Establishment of standards: Standards in the assessment and report of the characteristics of different NPs, including brightness, specificity, and toxicity, should be developed, set, and accepted community-wide in order to afford a fair and reliable comparison between different systems. With these standards in place, the research community will be able to compare the new generation of luminescent NPs rigorously and quantitatively, ranking luminescent NPs not only based on their intrinsic characteristics, but also weighing the use of such contrast agents for each specific tissue.
- Improvement of nanoparticle interbatch reproducibility: This goal is closely related to the previous objective because the features of luminescent NPs of a given material should not differ from batch to batch. Their performance should not depend on *who* fabricated them, once the synthesis protocol is officially established. In pursuit of reproducibility, the use of robots, automatization of the synthesis processes, and machine learning will prove fundamental.[241,242]
- Development of effective functionalization: As far as contrast agents are concerned, nontoxic, high-brightness NPs that emit light within carefully chosen spectral ranges are ultimately worthless if they do not reach the desired organ. The NPs specifically have to reach the site of interest, accumulate in substantial number, and reside long enough at the site to have real applicative potential. This process requires advanced surface functionalization that should be accompanied by a thorough understanding of how a NP interacts with cells and tissues at the *in vivo* level. With *in vitro* experiments, researchers have often been too optimistic when evaluating the targeting efficiency of functionalized NPs.

For all of the steps above, great support is to be expected from AI. Although still relatively in its infancy in many of the subfields discussed so far, the use of deep learning based on neural networks is envisaged to reduce the time consumed with trial-and-error approaches drastically by supporting a more rational design of contrast agents.

https://dx.doi.org/10.1021/acsnano.0c08349
ACS Nano 2021, 15, 1917−1941

After setting the boundaries above, we split our outlook of the realistic chances for a broader use of luminescent NPs for *in vivo* imaging between two different contexts: small-animal imaging for research purposes (preclinical) and applications in humans for disease detection (clinical), facilitating diagnosis or image-assisted therapies.

At the *preclinical* level, NP-enabled *in vivo* fluorescence imaging is already a reality in the imaging facilities of research institutions around the globe. However, we note that there are two steps yet to be taken to place fluorescence imaging at the same level as PET, MRI, PA, and CT. Luminescent NPs as contrast agents for *in vivo* imaging are often considered to be one echelon below small organic (fluorescent) molecules. High brightness (which is ultimately conducive to low injected doses), well-known clearance paths, and minimal related toxicity, along with knowledge of ways to engineer the fluorophore chemically, are the prominent reasons for preferring small molecules in this context. However, we argue that this preference is also the fruit of habit (*i.e.*, years of consolidated use of small molecules). For the forthcoming generation of luminescent NPs to become a viable option compared to such an established competitor, further progress in terms of brightness, certainty about the lack of toxicity, and clearance are key. On the positive side, luminescent NPs overpower small molecules in terms of emission tunability (easily reaching BW-II/BW-III emission, narrow emission, large Stokes shift) and long photoluminescence lifetimes. This latter characteristic affords the implementation of time-gated detection approaches, which alleviate the issues related with autofluorescence.

Irrespective of the chosen contrast agent, *in vivo* fluorescence imaging at the preclinical level has not yet been fully exploited. Specifically, the best of what fluorescence imaging has to offer in terms of real-time monitoring (*e.g.*, of metabolic processes) is yet to come. Moreover, based on the continuous improvement of infrared-emitting NPs and of BW-II/BW-III detection systems, we expect that whole-body 3D fluorescence imaging of small animals (which we identified as the future of preclinical fluorescence imaging) will be achieved within the next decade.

The future of *clinical* fluorescence imaging deserves more elaborate analysis, as it is a more complex and multifaceted scenario. In the discussion below, we primarily cite works related to QDs/semiconductors nanocrystals as examples of the proven applicability of NP-enabled fluorescence imaging. We do not wish to imply that other luminescent NPs could not pass the bar for clinical applications anytime soon, but research in semiconductor-based nanomaterials is currently providing the most promising results.

According to what we presented in this Perspective, the number of organs that are accessible *via* NP-enabled fluorescence imaging is relatively limited. As a result, it is highly unlikely that this imaging method could ever replace techniques that are capable of seeing deeper within the human body. However, for the set of tissues that can be observed *via* fluorescence imaging (skin, breast tissue, muscles, joints, brain surface), this simple, fast, and inexpensive diagnostic tool is expected to make its way to the clinic. This result will be achieved by working along the lines highlighted for achieving whole-body 3D imaging at the preclinical level in terms of better NPs, detection systems, and image reconstruction *via* the use of algorithms.

As we mentioned, the physical constraints regarding the applicability of fluorescence imaging in humans are relaxed in infants, owing to the intrinsic reduced size of organs and tissues. However, this increased accessibility is countered by more stringent requirements to be met from a safety viewpoint.

If we are willing to yield in part the noninvasiveness promised by NP-enabled fluorescence imaging, however, the horizon broadens. Indeed, fluorescence imaging is approved for clinical use in endoscopic and surgery-related applications. For endoscopic fluorescence imaging, optical fibers or, better, bundles of them are incorporated in the endoscopic probe.[243] This configuration enables clinicians to reach tissues at depths that prevent the employment of the less invasive approach of external illumination/collection of the fluorescence signal. Autofluorescence and/or emission of small dyes acting as markers can be leveraged to obtain information on the status of the tissue.[244−248] Although this endoscopic approach can only be used for diagnostic purposes, it is a powerful weapon in real-time fluorescence imaging of tumoral areas during surgeries. The ability to visualize the tumoral mass clearly and in real time prevents removal of unaffected tissue and helps ensure that the entirety of the tumoral mass is removed, thus averting recurrence. In that context, fluorescence imaging provides both high sensitivity and remarkable resolution (1 μm), but is hampered by the non-ideal properties of fluorophores currently approved for oncologic indications. The three fluorescent dyes currently approved by the FDA for cancer imaging are 5-aminolevulinic acid (for fluorescence-guided surgery), methylene blue (for sentinel lymph node mapping), and indocyanine green (for intraoperative tumor identification).[249−251] These molecules, to different degrees, exhibit nonspecific tissue distribution, lack of stability, possible toxic side effects, and excitation/emission at wavelengths that are not transmitted efficiently within tissues. In addition, because all three are small-molecule dyes, they are cleared quickly by the lymphatic system.[252−256]

Imaging-assisted surgery would ultimately benefit from preferring luminescent NPs over small organic dyes. Enlarging the picture, luminescent NPs can also be flexibly engineered to achieve longer retention times and more efficient tumor targeting, to provide multimodal imaging readouts and, arguably, to lead the way toward supplying nonmorphological data.[257−261] We anticipate that luminescent NPs will rival dye-based probes in clinical applications of fluorescence imaging within the next decade.

We anticipate that luminescent nanoparticles will rival dye-based probes in clinical applications of fluorescence imaging within the next decade.

To conclude, NP-enabled fluorescence imaging has a bright future, and we foresee its increasingly widespread use for several preclinical and clinical purposes. With this Perspective, we attempted to provide guidelines for ensuring that the efforts in the field are not misplaced, thus enabling researchers to reach significant goals in a timely manner.

AUTHOR INFORMATION

Corresponding Authors

Daniel Jaque − *Fluorescence Imaging Group, Departamento de Física de Materiales, Facultad de Ciencias, Universidad Autónoma de Madrid, Madrid 28049, Spain; Nanobiology Group, Instituto Ramón y Cajal de Investigación Sanitaria*

https://dx.doi.org/10.1021/acsnano.0c08349
ACS Nano 2021, 15, 1917−1941

(IRYCIS), Madrid 28034, Spain; orcid.org/0000-0002-3225-0667; Email: daniel.jaque@uam.es

Riccardo Marin − *Fluorescence Imaging Group, Departamento de Fısica de Materiales, Facultad de Ciencias, Universidad Autónoma de Madrid, Madrid 28049, Spain;* orcid.org/0000-0003-3270-892X; Email: riccardo.marin@hotmail.it

Authors

Erving Ximendes − *Fluorescence Imaging Group, Departamento de Fısica de Materiales, Facultad de Ciencias, Universidad Autónoma de Madrid, Madrid 28049, Spain; Nanobiology Group, Instituto Ramón y Cajal de Investigación Sanitaria (IRYCIS), Madrid 28034, Spain;* orcid.org/0000-0001-7182-0573

Antonio Benayas − *Fluorescence Imaging Group, Departamento de Fısica de Materiales, Facultad de Ciencias, Universidad Autónoma de Madrid, Madrid 28049, Spain; Nanobiology Group, Instituto Ramón y Cajal de Investigación Sanitaria (IRYCIS), Madrid 28034, Spain*

Complete contact information is available at: https://pubs.acs.org/10.1021/acsnano.0c08349

Notes

The authors declare no competing financial interest.

ACKNOWLEDGMENTS

This work has been cofinanced by European Structural and Investment Fund and by the European Union's Horizon 2020 FET Open program under grant agreement no. 801305 (NanoTBTech). E.X. is grateful for a Juan de la Cierva Formación scholarship (FJC2018-036734-I). A.B. acknowledges funding from Comunidad de Madrid through TALENTO grant ref. 2019-T1/IND-14014. D.J. acknowledges the Ministerio de Economía y Competitividad-MINECO (MAT2016-75362-C3-1-R), the Ministerio de Ciencia e Innovacion of Spain (PID2019-106211RB-I00), and the Comunidad de Madrid (B2017/BMD-3867 RENIM-CM). R.M. acknowledges the support of the R.M. acknowledges the support of the European Commission through the Marie Skłodowska-Curie Grant no. 797945 (LANTERNS).

REFERENCES

(1) Throughout this paper, the term "light" is used interchangeably with "electromagnetic radiation" to refer indistinctly to the UV, visible and/or infrared part of the electromagnetic spectrum. We do so assuming a widely accepted informal consensus, although rigorously speaking "light" indicates only the visible range.

(2) Huang, D.; Swanson, E. A.; Lin, C. P.; Schuman, J. S.; Stinson, W. G.; Chang, W.; Hee, M. R.; Flotte, T.; Gregory, K.; Puliafito, C. A.; Fujimoto, J. G. Optical Coherence Tomography. *Science* **1991**, *254*, 1178−1181.

(3) Sevick-Muraca, E. M.; Lopez, G.; Reynolds, J. S.; Troy, T. L.; Hutchinson, C. L. Fluorescence and Absorption Contrast Mechanisms for Biomedical Optical Imaging Using Frequency-Domain Techniques. *Photochem. Photobiol.* **1997**, *66*, 55−64.

(4) Yuan, B.; Burgess, S. A.; Iranmahboob, A.; Bouchard, M. B.; Lehrer, N.; Bordier, C.; Hillman, E. M. A System for High-Resolution Depth-Resolved Optical Imaging of Fluorescence and Absorption Contrast. *Rev. Sci. Instrum.* **2009**, *80*, 043706.

(5) Marin, R.; Lifante, J.; Besteiro, L. V.; Wang, Z.; Govorov, A. O.; Rivero, F.; Alfonso, F.; Sanz-Rodriguez, F.; Jaque, D. Plasmonic Copper Sulfide Nanoparticles Enable Dark Contrast in Optical Coherence Tomography. *Adv. Healthcare Mater.* **2020**, *9*, No. 1901627.

(6) Liu, Y.; Bhattarai, P.; Dai, Z.; Chen, X. Photothermal Therapy and Photoacoustic Imaging *via* Nanotheranostics in Fighting Cancer. *Chem. Soc. Rev.* **2019**, *48*, 2053−2108.

(7) Abbaci, M.; Conversano, A.; De Leeuw, F.; Laplace-Builhe, C.; Mazouni, C. Near-Infrared Fluorescence Imaging for the Prevention and Management of Breast Cancer-Related Lymphedema: A Systematic Review. *Eur. J. Surg. Oncol.* **2019**, *45*, 1778−1786.

(8) Dsouza, A. V.; Lin, H.; Henderson, E. R.; Samkoe, K. S.; Pogue, B. W. Review of Fluorescence Guided Surgery Systems: Identification of Key Performance Capabilities Beyond Indocyanine Green Imaging. *J. Biomed. Opt.* **2016**, *21*, 080901.

(9) Weber, J.; Beard, P. C.; Bohndiek, S. E. Contrast Agents for Molecular Photoacoustic Imaging. *Nat. Methods* **2016**, *13*, 639−650.

(10) Jiang, Y.; Pu, K. Molecular Fluorescence and Photoacoustic Imaging in the Second Near-Infrared Optical Window Using Organic Contrast Agents. *Adv. Biosyst.* **2018**, *2*, 1700262.

(11) Kenry; Duan, Y.; Liu, B. Recent Advances of Optical Imaging in the Second Near-Infrared Window. *Adv. Mater.* **2018**, *30*, No. 1802394.

(12) Cole, A. J.; Yang, V. C.; David, A. E. Cancer Theranostics: The Rise of Targeted Magnetic Nanoparticles. *Trends Biotechnol.* **2011**, *29*, 323−332.

(13) Xie, J.; Lee, S.; Chen, X. Nanoparticle-Based Theranostic Agents. *Adv. Drug Delivery Rev.* **2010**, *62*, 1064−1079.

(14) Skripka, A.; Karabanovas, V.; Jarockyte, G.; Marin, R.; Tam, V.; Cerruti, M.; Rotomskis, R.; Vetrone, F. Decoupling Theranostics with Rare Earth Doped Nanoparticles. *Adv. Funct. Mater.* **2019**, *29*, 1807105.

(15) Schmitz-Valckenberg, S.; Lara, D.; Nizari, S.; Normando, E. M.; Guo, L.; Wegener, A. R.; Tufail, A.; Fitzke, F. W.; Holz, F. G.; Cordeiro, M. F. Localisation and Significance of *In Vivo* Near-Infrared Autofluorescent Signal in Retinal Imaging. *Br. J. Ophthalmol.* **2011**, *95*, 1134−1139.

(16) Croce, A. C.; Bottiroli, G. Autofluorescence Spectroscopy and Imaging: A Tool for Biomedical Research and Diagnosis. *Eur. J. Histochem.* **2014**, *58*, 2461.

(17) Jacques, S. L. Optical Properties of Biological Tissues: A Review. *Phys. Med. Biol.* **2013**, *58*, R37−61.

(18) Bashkatov, A. N.; Genina, E. A.; Kochubey, V. I.; Tuchin, V. V. Optical Properties of Human Skin, Subcutaneous and Mucous Tissues in the Wavelength Range from 400 to 2000 nm. *J. Phys. D: Appl. Phys.* **2005**, *38*, 2543−2555.

(19) Jaque, D.; Richard, C.; Viana, B.; Soga, K.; Liu, X.; García Solé, J. Inorganic Nanoparticles for Optical Bioimaging. *Adv. Opt. Photonics* **2016**, *8*, 1−103.

(20) Reisz, J. A.; Bansal, N.; Qian, J.; Zhao, W.; Furdui, C. M. Effects of Ionizing Radiation on Biological Molecules—Mechanisms of Damage and Emerging Methods of Detection. *Antioxid. Redox Signaling* **2014**, *21*, 260−292.

(21) Lee, D.-E.; Koo, H.; Sun, I.-C.; Ryu, J. H.; Kim, K.; Kwon, I. C. Multifunctional Nanoparticles for Multimodal Imaging and Theragnosis. *Chem. Soc. Rev.* **2012**, *41*, 2656−2672.

(22) Sharma, P.; Brown, S.; Walter, G.; Santra, S.; Moudgil, B. Nanoparticles for Bioimaging. *Adv. Colloid Interface Sci.* **2006**, *123*−*126*, 471−485.

(23) Mout, R.; Moyano, D. F.; Rana, S.; Rotello, V. M. Surface Functionalization of Nanoparticles for Nanomedicine. *Chem. Soc. Rev.* **2012**, *41*, 2539−2544.

(24) Villa, I.; Vedda, A.; Cantarelli, I. X.; Pedroni, M.; Piccinelli, F.; Bettinelli, M.; Speghini, A.; Quintanilla, M.; Vetrone, F.; Rocha, U.; Jacinto, C.; Carrasco, E.; Rodríguez, F. S.; Juarranz, Á.; del Rosal, B.; Ortgies, D. H.; Gonzalez, P. H.; Solé, J. G.; García, D. J. 1.3 μm Emitting SrF_2:Nd^{3+} Nanoparticles for High Contrast *In Vivo* Imaging in the Second Biological Window. *Nano Res.* **2015**, *8*, 649−665.

(25) Diao, S.; Hong, G.; Antaris, A. L.; Blackburn, J. L.; Cheng, K.; Cheng, Z.; Dai, H. Biological Imaging Without Autofluorescence in the Second Near-Infrared Region. *Nano Res.* **2015**, *8*, 3027−3034.

(26) Smith, A. M.; Mancini, M. C.; Nie, S. Bioimaging: Second Window for *In Vivo* Imaging. *Nat. Nanotechnol.* **2009**, *4*, 710−711.

(27) Hemmer, E.; Benayas, A.; Legare, F.; Vetrone, F. Exploiting the Biological Windows: Current Perspectives on Fluorescent Bioprobes Emitting above 1000 nm. *Nanoscale Horiz.* **2016**, *1*, 168−184.
(28) Welsher, K.; Sherlock, S. P.; Dai, H. Deep-Tissue Anatomical Imaging of Mice Using Carbon Nanotube Fluorophores in the Second Near-Infrared Window. *Proc. Natl. Acad. Sci. U. S. A.* **2011**, *108*, 8943−8948.
(29) Naczynski, D. J.; Tan, M. C.; Zevon, M.; Wall, B.; Kohl, J.; Kulesa, A.; Chen, S.; Roth, C. M.; Riman, R. E.; Moghe, P. V. Rare-Earth-Doped Biological Composites as *In Vivo* Shortwave Infrared Reporters. *Nat. Commun.* **2013**, *4*, 2199.
(30) Hong, G.; Robinson, J. T.; Zhang, Y.; Diao, S.; Antaris, A. L.; Wang, Q.; Dai, H. *In Vivo* Fluorescence Imaging with Ag_2S Quantum Dots in the Second Near-Infrared Region. *Angew. Chem., Int. Ed.* **2012**, *51*, 9818−9821.
(31) Zhang, Y.; Hong, G.; Zhang, Y.; Chen, G.; Li, F.; Dai, H.; Wang, Q. Ag_2S Quantum Dot: A Bright and Biocompatible Fluorescent Nanoprobe in the Second Near-Infrared Window. *ACS Nano* **2012**, *6*, 3695−3702.
(32) Angelo, J.; Chen, S.-J.; Ochoa, M.; Sunar, U.; Gioux, S.; Intes, X. Review of Structured Light in Diffuse Optical Imaging. *J. Biomed. Opt.* **2019**, *24*, 071602.
(33) Umezawa, M.; Sera, T.; Yokota, H.; Takematsu, M.; Morita, M.; Yeroslavsky, G.; Kamimura, M.; Soga, K. Computed Tomography for In Vivo Deep Over-1000 nm Near-Infrared Fluorescence Imaging. *J. Biophotonics* **2020**, *13*, No. e202000071.
(34) Zhong, Y.; Ma, Z.; Zhu, S.; Yue, J.; Zhang, M.; Antaris, A. L.; Yuan, J.; Cui, R.; Wan, H.; Zhou, Y.; Wang, W.; Huang, N. F.; Luo, J.; Hu, Z.; Dai, H. Boosting the Down-Shifting Luminescence of Rare-Earth Nanocrystals for Biological Imaging Beyond 1500 nm. *Nat. Commun.* **2017**, *8*, 737.
(35) Santos, H. D. A.; Zabala Gutierrez, I.; Shen, Y.; Lifante, J.; Ximendes, E.; Laurenti, M.; Mendez-Gonzalez, D.; Melle, S.; Calderon, O. G.; Lopez Cabarcos, E.; Fernandez, N.; Chaves-Coira, I.; Lucena-Agell, D.; Monge, L.; Mackenzie, M. D.; Marques-Hueso, J.; Jones, C. M. S.; Jacinto, C.; Del Rosal, B.; Kar, A. K.; et al. Ultrafast Photochemistry Produces Superbright Short-Wave Infrared Dots for Low-Dose *In Vivo* Imaging. *Nat. Commun.* **2020**, *11*, 2933.
(36) Li, C.; Zhang, Y.; Wang, M.; Zhang, Y.; Chen, G.; Li, L.; Wu, D.; Wang, Q. *In Vivo* Real-Time Visualization of Tissue Blood Flow and Angiogenesis Using Ag_2S Quantum Dots in the NIR-II Window. *Biomaterials* **2014**, *35*, 393−400.
(37) Bruns, O. T.; Bischof, T. S.; Harris, D. K.; Franke, D.; Shi, Y.; Riedemann, L.; Bartelt, A.; Jaworski, F. B.; Carr, J. A.; Rowlands, C. J.; Wilson, M. W. B.; Chen, O.; Wei, H.; Hwang, G. W.; Montana, D. M.; Coropceanu, I.; Achorn, O. B.; Kloepper, J.; Heeren, J.; So, P. T. C.; et al. Next-Generation *In Vivo* Optical Imaging with Short-Wave Infrared Quantum Dots. *Nat. Biomed. Eng.* **2017**, *1*, 0056.
(38) Peng, P.; Wu, N.; Ye, L.; Jiang, F.; Feng, W.; Li, F.; Liu, Y.; Hong, M. Biodegradable Inorganic Upconversion Nanocrystals for *in Vivo* Applications. *ACS Nano* **2020**, *14*, 16672−16680.
(39) Lisjak, D.; Plohl, O.; Vidmar, J.; Majaron, B.; Ponikvar-Svet, M. Dissolution Mechanism of Upconverting AYF_4:Yb,Tm (A = Na or K) Nanoparticles in Aqueous Media. *Langmuir* **2016**, *32*, 8222−8229.
(40) Palo, E.; Zhang, H.; Lastusaari, M.; Salomäki, M. Nanometer-Thick Ion-Selective Polyelectrolyte Multilayer Coatings To Inhibit the Disintegration of Inorganic Upconverting Nanoparticles. *ACS Appl. Nano Mater.* **2020**, *3*, 6892−6898.
(41) Lahtinen, S.; Lyytikäinen, A.; Päkkilä, H.; Hömppi, E.; Perälä, N.; Lastusaari, M.; Soukka, T. Disintegration of Hexagonal $NaYF_4$:Yb^{3+},Er^{3+} Upconverting Nanoparticles in Aqueous Media: The Role of Fluoride in Solubility Equilibrium. *J. Phys. Chem. C* **2017**, *121*, 656−665.
(42) Plohl, O.; Kraft, M.; Kovac, J.; Belec, B.; Ponikvar-Svet, M.; Wurth, C.; Lisjak, D.; Resch-Genger, U. Optically Detected Degradation of $NaYF_4$:Yb,Tm-Based Upconversion Nanoparticles in Phosphate Buffered Saline Solution. *Langmuir* **2017**, *33*, 553−560.
(43) De Jong, W. H.; Hagens, W. I.; Krystek, P.; Burger, M. C.; Sips, A. J.; Geertsma, R. E. Particle Size-Dependent Organ Distribution of Gold Nanoparticles After Intravenous Administration. *Biomaterials* **2008**, *29*, 1912−1919.
(44) Mijnendonckx, K.; Leys, N.; Mahillon, J.; Silver, S.; Van Houdt, R. Antimicrobial Silver: Uses, Toxicity and Potential for Resistance. *BioMetals* **2013**, *26*, 609−621.
(45) Gaetke, L. Copper Toxicity, Oxidative Stress, and Antioxidant Nutrients. *Toxicology* **2003**, *189*, 147−163.
(46) Zhang, Y. N.; Poon, W.; Tavares, A. J.; McGilvray, I. D.; Chan, W. C. W. Nanoparticle-Liver Interactions: Cellular Uptake and Hepatobiliary Elimination. *J. Controlled Release* **2016**, *240*, 332−348.
(47) Boey, A.; Ho, H. K. All Roads Lead to the Liver: Metal Nanoparticles and their Implications for Liver Health. *Small* **2020**, *16*, No. 2000153.
(48) Poon, W.; Zhang, Y. N.; Ouyang, B.; Kingston, B. R.; Wu, J. L. Y.; Wilhelm, S.; Chan, W. C. W. Elimination Pathways of Nanoparticles. *ACS Nano* **2019**, *13*, 5785−5798.
(49) Ermolin, M. S.; Fedotov, P. S.; Malik, N. A.; Karandashev, V. K. Nanoparticles of Volcanic Ash as a Carrier for Toxic Elements on the Global Scale. *Chemosphere* **2018**, *200*, 16−22.
(50) Yang, Y.; Vance, M.; Tou, F.; Tiwari, A.; Liu, M.; Hochella, M. F. Nanoparticles in Road Dust from Impervious Urban Surfaces: Distribution, Identification, and Environmental Implications. *Environ. Sci.: Nano* **2016**, *3*, 534−544.
(51) Uebe, R.; Schuler, D. Magnetosome Biogenesis in Magnetotactic Bacteria. *Nat. Rev. Microbiol.* **2016**, *14*, 621−637.
(52) Jayaweera, M.; Perera, H.; Gunawardana, B.; Manatunge, J. Transmission of COVID-19 Virus by Droplets and Aerosols: A Critical Review on the Unresolved Dichotomy. *Environ. Res.* **2020**, *188*, 109819.
(53) Donaldson, K.; Stone, V.; Tran, C. L.; Kreyling, W.; Borm, P. J. Nanotoxicology. *Occup. Environ. Med.* **2004**, *61*, 727−728.
(54) Wilsdon, J. The Politics of Small Things: Nanotechnology, Risk, and Uncertainty. *IEEE Technol. Soc. Mag.* **2004**, *23*, 16−21.
(55) Colvin, V. L. The Potential Environmental Impact of Engineered Nanomaterials. *Nat. Biotechnol.* **2003**, *21*, 1166−1170.
(56) Jani, P.; Halbert, G. W.; Langridge, J.; Florence, A. T. Nanoparticle Uptake by the Rat Gastrointestinal Mucosa: Quantitation and Particle Size Dependency. *J. Pharm. Pharmacol.* **1990**, *42*, 821−826.
(57) Utell, M. J.; Frampton, M. W. Acute Health Effects of Ambient Air Pollution: The Ultrafine Particle Hypothesis. *J. Aerosol Med.* **2000**, *13*, 355−359.
(58) Ferin, J.; Oberdörster, G. Translocation of Particles from Pulmonary Alveoli into the Interstitium*. *J. Aerosol Med.* **1992**, *5*, 179−187.
(59) Tan, M. H.; Commens, C. A.; Burnett, L.; Snitch, P. J. A Pilot Study on the Percutaneous Absorption of Microfine Titanium Dioxide from Sunscreens. *Australas. J. Dermatol.* **1996**, *37*, 185−187.
(60) Oberdörster, G.; Utell, M. J. Ultrafine Particles in the Urban Air: To the Respiratory Tract—and Beyond? *Environ. Health. Perspect.* **2002**, *110*, A440−A441.
(61) Choi, H. S.; Ashitate, Y.; Lee, J. H.; Kim, S. H.; Matsui, A.; Insin, N.; Bawendi, M. G.; Semmler-Behnke, M.; Frangioni, J. V.; Tsuda, A. Rapid Translocation of Nanoparticles from the Lung Airspaces to the Body. *Nat. Biotechnol.* **2010**, *28*, 1300−1303.
(62) Kreyling, W. G.; Hirn, S.; Schleh, C. Nanoparticles in the Lung. *Nat. Biotechnol.* **2010**, *28*, 1275−1276.
(63) Hagens, W. I.; Oomen, A. G.; de Jong, W. H.; Cassee, F. R.; Sips, A. J. What Do We (Need To) Know About the Kinetic Properties of Nanoparticles in the Body? *Regul. Toxicol. Pharmacol.* **2007**, *49*, 217−229.
(64) Ban, Z.; Zhou, Q.; Sun, A.; Mu, L.; Hu, X. Screening Priority Factors Determining and Predicting the Reproductive Toxicity of Various Nanoparticles. *Environ. Sci. Technol.* **2018**, *52*, 9666−9676.
(65) Millstone, J. E.; Chan, W. C. W.; Kagan, C. R.; Liz-Marzan, L. M.; Kotov, N. A.; Mulvaney, P. A.; Parak, W. J.; Rogach, A. L.; Weiss, P. S.; Schaak, R. E. Redefining the Experimental and Methods Sections. *ACS Nano* **2019**, *13*, 4862−4864.
(66) Join the Dialogue. *Nat. Nanotechnol.* **2012**, *7*, 545.
(67) Lammers, T.; Storm, G. Setting Standards To Promote Progress in Bio-Nano Science. *Nat. Nanotechnol.* **2019**, *14*, 626.

https://dx.doi.org/10.1021/acsnano.0c08349
ACS Nano 2021, 15, 1917−1941

(68) Faria, M.; Bjornmalm, M.; Thurecht, K. J.; Kent, S. J.; Parton, R. G.; Kavallaris, M.; Johnston, A. P. R.; Gooding, J. J.; Corrie, S. R.; Boyd, B. J.; Thordarson, P.; Whittaker, A. K.; Stevens, M. M.; Prestidge, C. A.; Porter, C. J. H.; Parak, W. J.; Davis, T. P.; Crampin, E. J.; Caruso, F. Minimum Information Reporting in Bio-Nano Experimental Literature. *Nat. Nanotechnol.* **2018**, *13*, 777−785.
(69) Leong, H. S.; Butler, K. S.; Brinker, C. J.; Azzawi, M.; Conlan, S.; Dufes, C.; Owen, A.; Rannard, S.; Scott, C.; Chen, C.; Dobrovolskaia, M. A.; Kozlov, S. V.; Prina-Mello, A.; Schmid, R.; Wick, P.; Caputo, F.; Boisseau, P.; Crist, R. M.; McNeil, S. E.; Fadeel, B.; et al. On the Issue of Transparency and Reproducibility in Nanomedicine. *Nat. Nanotechnol.* **2019**, *14*, 629−635.
(70) Winkler, D. A.; Mombelli, E.; Pietroiusti, A.; Tran, L.; Worth, A.; Fadeel, B.; McCall, M. J. Applying Quantitative Structure-Activity Relationship Approaches to Nanotoxicology: Current Status and Future Potential. *Toxicology* **2013**, *313*, 15−23.
(71) Lazarovits, J.; Sindhwani, S.; Tavares, A. J.; Zhang, Y.; Song, F.; Audet, J.; Krieger, J. R.; Syed, A. M.; Stordy, B.; Chan, W. C. W. Supervised Learning and Mass Spectrometry Predicts the *in Vivo* Fate of Nanomaterials. *ACS Nano* **2019**, *13*, 8023−8034.
(72) https://eur-lex.europa.eu/legal-content/EN/ALL/?uri=CELEX:32000L0053 (accessed 2020-10-08).
(73) https://ec.europa.eu/commission/presscorner/detail/en/IP_06_903 (accessed 2020-10-08).
(74) Hanifi, D. A.; Bronstein, N. D.; Koscher, B. A.; Nett, Z.; Swabeck, J. K.; Takano, K.; Schwartzberg, A. M.; Maserati, L.; Vandewal, K.; van de Burgt, Y.; Salleo, A.; Alivisatos, A. P. Redefining Near-Unity Luminescence in Quantum Dots with Photothermal Threshold Quantum Yield. *Science* **2019**, *363*, 1199−1202.
(75) Benayas, A.; Ren, F.; Carrasco, E.; Marzal, V.; del Rosal, B.; Gonfa, B. A.; Juarranz, Á.; Sanz-Rodríguez, F.; Jaque, D.; García-Solé, J.; Ma, D.; Vetrone, F. PbS/CdS/ZnS Quantum Dots: A Multifunctional Platform for *In Vivo* Near-Infrared Low-Dose Fluorescence Imaging. *Adv. Funct. Mater.* **2015**, *25*, 6650−6659.
(76) https://ec.europa.eu/info/law/better-regulation/have-your-say/initiatives/11802-Exemptions-to-End-of-life-vehicle-ELV-Directive-9th-amendment (accessed 2020-10-08).
(77) Liu, Y.; Tourbin, M.; Lachaize, S.; Guiraud, P. Nanoparticles in Wastewaters: Hazards, Fate and Remediation. *Powder Technol.* **2014**, *255*, 149−156.
(78) Rim, K. T.; Koo, K. H.; Park, J. S. Toxicological Evaluations of Rare Earths and their Health Impacts to Workers: A Literature Review. *SH W* **2013**, *4*, 12−26.
(79) Gnach, A.; Lipinski, T.; Bednarkiewicz, A.; Rybka, J.; Capobianco, J. A. Upconverting Nanoparticles: Assessing the Toxicity. *Chem. Soc. Rev.* **2015**, *44*, 1561−1584.
(80) Cotruvo, J. A., Jr The Chemistry of Lanthanides in Biology: Recent Discoveries, Emerging Principles, and Technological Applications. *ACS Cent. Sci.* **2019**, *5*, 1496−1506.
(81) Zhang, M.; Yue, J.; Cui, R.; Ma, Z.; Wan, H.; Wang, F.; Zhu, S.; Zhou, Y.; Kuang, Y.; Zhong, Y.; Pang, D. W.; Dai, H. Bright Quantum Dots Emitting at Approximately 1,600 nm in the NIR-IIb Window for Deep Tissue Fluorescence Imaging. *Proc. Natl. Acad. Sci. U. S. A.* **2018**, *115*, 6590−6595.
(82) Chen, J.; Kong, Y.; Wang, W.; Fang, H.; Wo, Y.; Zhou, D.; Wu, Z.; Li, Y.; Chen, S. Direct Water-Phase Synthesis of Lead Sulfide Quantum Dots Encapsulated by Beta-Lactoglobulin for *In Vivo* Second Near Infrared Window Imaging with Reduced Toxicity. *Chem. Commun.* **2016**, *52*, 4025−4028.
(83) Shi, X.; Chen, S.; Luo, M.-Y.; Huang, B.; Zhang, G.; Cui, R.; Zhang, M. Zn-Doping Enhances the Photoluminescence and Stability of PbS Quantum Dots for *In Vivo* High-Resolution Imaging in the NIR-II Window. *Nano Res.* **2020**, *13*, 2239−2245.
(84) Wang, D.; Qian, J.; Cai, F.; He, S.; Han, S.; Mu, Y. 'Green'-Synthesized Near-Infrared PbS Quantum Dots with Silica-PEG Dual-Layer Coating: Ultrastable and Biocompatible Optical Probes for *In Vivo* Animal Imaging. *Nanotechnology* **2012**, *23*, 245701.
(85) Hu, R.; Law, W. C.; Lin, G.; Ye, L.; Liu, J.; Liu, J.; Reynolds, J. L.; Yong, K. T. PEGylated Phospholipid Micelle-Encapsulated Near-Infrared PbS Quantum Dots for *In Vitro* and *In Vivo* Bioimaging. *Theranostics* **2012**, *2*, 723−733.
(86) Kong, Y.; Chen, J.; Fang, H.; Heath, G.; Wo, Y.; Wang, W.; Li, Y.; Guo, Y.; Evans, S. D.; Chen, S.; Zhou, D. Highly Fluorescent Ribonuclease-A-Encapsulated Lead Sulfide Quantum Dots for Ultrasensitive Fluorescence in Vivo Imaging in the Second Near-Infrared Window. *Chem. Mater.* **2016**, *28* (9), 3041−3050.
(87) Zamberlan, F.; Turyanska, L.; Patane, A.; Liu, Z.; Williams, H. E. L.; Fay, M. W.; Clarke, P. A.; Imamura, Y.; Jin, T.; Bradshaw, T. D.; Thomas, N. R.; Grabowska, A. M. Stable DHLA-PEG capped PbS quantum dots: from synthesis to near-infrared biomedical imaging. *J. Mater. Chem. B* **2018**, *6* (4), 550−555.
(88) Qiu, X.; Zhu, X.; Su, X.; Xu, M.; Yuan, W.; Liu, Q.; Xue, M.; Liu, Y.; Feng, W.; Li, F. Near-Infrared Upconversion Luminescence and Bioimaging *In Vivo* Based on Quantum Dots. *Adv. Sci.* **2019**, *6*, 1801834.
(89) Dabbousi, B. O.; Rodriguez-Viejo, J.; Mikulec, F. V.; Heine, J. R.; Mattoussi, H.; Ober, R.; Jensen, K. F.; Bawendi, M. G. (CdSe)ZnS Core-Shell Quantum Dots: Synthesis and Characterization of a Size Series of Highly Luminescent Nanocrystallites. *J. Phys. Chem. B* **1997**, *101*, 9463−9475.
(90) Chen, G.; Shen, J.; Ohulchanskyy, T. Y.; Patel, N. J.; Kutikov, A.; Li, Z.; Song, J.; Pandey, R. K.; Agren, H.; Prasad, P. N.; Han, G. (α-$NaYbF_4$:Tm^{3+})/CaF_2 Core/Shell Nanoparticles with Efficient Near-Infrared to Near-Infrared Upconversion for High-Contrast Deep Tissue Bioimaging. *ACS Nano* **2012**, *6*, 8280−8287.
(91) Ding, H.; Zhou, X.; Qin, B.; Zhou, Z.; Zhao, Y. Highly Fluorescent Near-Infrared Emitting Carbon Dots Derived from Lemon Juice and its Bioimaging Application. *J. Lumin.* **2019**, *211*, 298−304.
(92) Bao, X.; Yuan, Y.; Chen, J.; Zhang, B.; Li, D.; Zhou, D.; Jing, P.; Xu, G.; Wang, Y.; Hola, K.; Shen, D.; Wu, C.; Song, L.; Liu, C.; Zboril, R.; Qu, S. *In Vivo* Theranostics with Near-Infrared-Emitting Carbon Dots-Highly Efficient Photothermal Therapy Based on Passive Targeting After Intravenous Administration. *Light: Sci. Appl.* **2018**, *7*, 91.
(93) Ding, H.; Yu, S. B.; Wei, J. S.; Xiong, H. M. Full-Color Light-Emitting Carbon Dots with a Surface-State-Controlled Luminescence Mechanism. *ACS Nano* **2016**, *10*, 484−491.
(94) Bian, W.; Lin, Y.; Wang, T.; Yu, X.; Qiu, J.; Zhou, M.; Luo, H.; Yu, S. F.; Xu, X. Direct Identification of Surface Defects and their Influence on the Optical Characteristics of Upconversion Nanoparticles. *ACS Nano* **2018**, *12*, 3623−3628.
(95) Rivest, J. B.; Jain, P. K. Cation Exchange on the Nanoscale: An Emerging Technique for New Material Synthesis, Device Fabrication, and Chemical Sensing. *Chem. Soc. Rev.* **2013**, *42*, 89−96.
(96) Bogdan, N.; Vetrone, F.; Ozin, G. A.; Capobianco, J. A. Synthesis of Ligand-Free Colloidally Stable Water Dispersible Brightly Luminescent Lanthanide-Doped Upconverting Nanoparticles. *Nano Lett.* **2011**, *11*, 835−840.
(97) Ivask, A.; Kurvet, I.; Kasemets, K.; Blinova, I.; Aruoja, V.; Suppi, S.; Vija, H.; Kakinen, A.; Titma, T.; Heinlaan, M.; Visnapuu, M.; Koller, D.; Kisand, V.; Kahru, A. Size-Dependent Toxicity of Silver Nanoparticles to Bacteria, Yeast, Algae, Crustaceans and Mammalian Cells *in Vitro*. *PLoS One* **2014**, *9*, No. e102108.
(98) Senut, M. C.; Zhang, Y.; Liu, F.; Sen, A.; Ruden, D. M.; Mao, G. Size-Dependent Toxicity of Gold Nanoparticles on Human Embryonic Stem Cells and their Neural Derivatives. *Small* **2016**, *12*, 631−646.
(99) Karlsson, H. L.; Gustafsson, J.; Cronholm, P.; Moller, L. Size-Dependent Toxicity of Metal Oxide Particles—A Comparison Between Nano- and Micrometer Size. *Toxicol. Lett.* **2009**, *188*, 112−118.
(100) Betzer, O.; Shilo, M.; Opochinsky, R.; Barnoy, E.; Motiei, M.; Okun, E.; Yadid, G.; Popovtzer, R. The Effect of Nanoparticle Size on the Ability To Cross the Blood-Brain Barrier: An *in Vivo* Study. *Nanomedicine* **2017**, *12*, 1533−1546.
(101) Gao, K.; Jiang, X. Influence of Particle Size on Transport of Methotrexate Across Blood Brain Barrier by Polysorbate 80-Coated Polybutylcyanoacrylate Nanoparticles. *Int. J. Pharm.* **2006**, *310*, 213−219.

https://dx.doi.org/10.1021/acsnano.0c08349
ACS Nano 2021, 15, 1917−1941

(102) Guo, Y.; Terazzi, E.; Seemann, R.; Fleury, J. B.; Baulin, V. A. Direct Proof of Spontaneous Translocation of Lipid-Covered Hydrophobic Nanoparticles Through a Phospholipid Bilayer. *Sci. Adv.* **2016**, *2*, No. e1600261.
(103) Villanueva-Flores, F.; Castro-Lugo, A.; Ramirez, O. T.; Palomares, L. A. Understanding Cellular Interactions with Nanomaterials: Towards a Rational Design of Medical Nanodevices. *Nanotechnology* **2020**, *31*, 132002.
(104) Singh, R. P.; Das, M.; Thakare, V.; Jain, S. Functionalization Density Dependent Toxicity of Oxidized Multiwalled Carbon Nanotubes in a Murine Macrophage Cell Line. *Chem. Res. Toxicol.* **2012**, *25*, 2127−2137.
(105) Albanese, A.; Chan, W. C. Effect of Gold Nanoparticle Aggregation on Cell Uptake and Toxicity. *ACS Nano* **2011**, *5*, 5478−5489.
(106) Yang, J. A.; Lohse, S. E.; Murphy, C. J. Tuning Cellular Response to Nanoparticles *via* Surface Chemistry and Aggregation. *Small* **2014**, *10*, 1642−1651.
(107) Tripathy, N.; Hong, T. K.; Ha, K. T.; Jeong, H. S.; Hahn, Y. B. Effect of ZnO Nanoparticles Aggregation on the Toxicity in RAW 264.7 Murine Macrophage. *J. Hazard. Mater.* **2014**, *270*, 110−117.
(108) Liu, X.; Chen, Y.; Li, H.; Huang, N.; Jin, Q.; Ren, K.; Ji, J. Enhanced Retention and Cellular Uptake of Nanoparticles in Tumors by Controlling their Aggregation Behavior. *ACS Nano* **2013**, *7*, 6244−6257.
(109) Li, H.; Chen, Y.; Li, Z.; Li, X.; Jin, Q.; Ji, J. Hemoglobin as a Smart pH-Sensitive Nanocarrier To Achieve Aggregation Enhanced Tumor Retention. *Biomacromolecules* **2018**, *19*, 2007−2013.
(110) Qian, R. C.; Lv, J.; Long, Y. T. Controllable Aggregation-Induced Exocytosis Inhibition (CAIEI) of Plasmonic Nanoparticles in Cancer Cells Regulated by MicroRNA. *Mol. Pharmaceutics* **2018**, *15*, 4031−4037.
(111) Nair, S.; Sasidharan, A.; Divya Rani, V. V.; Menon, D.; Nair, S.; Manzoor, K.; Raina, S. Role of Size Scale of ZnO Nanoparticles and Microparticles on Toxicity Toward Bacteria and Osteoblast Cancer Cells. *J. Mater. Sci.: Mater. Med.* **2009**, *20* (1), 235−241.
(112) Poland, C. A.; Duffin, R.; Kinloch, I.; Maynard, A.; Wallace, W. A.; Seaton, A.; Stone, V.; Brown, S.; Macnee, W.; Donaldson, K. Carbon Nanotubes Introduced Into the Abdominal Cavity of Mice Show Asbestos-Like Pathogenicity in a Pilot Study. *Nat. Nanotechnol.* **2008**, *3*, 423−428.
(113) Harik, V. M. Geometry of Carbon Nanotubes and Mechanisms of Phagocytosis and Toxic Effects. *Toxicol. Lett.* **2017**, *273*, 69−85.
(114) Liu, Y.; Zhao, Y.; Sun, B.; Chen, C. Understanding the Toxicity of Carbon Nanotubes. *Acc. Chem. Res.* **2013**, *46*, 702−713.
(115) Muller, J.; Huaux, F.; Moreau, N.; Misson, P.; Heilier, J. F.; Delos, M.; Arras, M.; Fonseca, A.; Nagy, J. B.; Lison, D. Respiratory Toxicity of Multi-Wall Carbon Nanotubes. *Toxicol. Appl. Pharmacol.* **2005**, *207*, 221−231.
(116) Sun, H.; Jiang, C.; Wu, L.; Bai, X.; Zhai, S. Cytotoxicity-Related Bioeffects Induced by Nanoparticles: The Role of Surface Chemistry. *Front. Bioeng. Biotechnol.* **2019**, *7*, 414.
(117) Lin, G.; Chen, T.; Pan, Y.; Yang, Z.; Li, L.; Yong, K. T.; Wang, X.; Wang, J.; Chen, Y.; Jiang, W.; Weng, S.; Huang, X.; Kuang, J.; Xu, G. Biodistribution and Acute Toxicity of Cadmium-Free Quantum Dots with Different Surface Functional Groups in Mice Following Intratracheal Inhalation. *Nanotheranostics* **2020**, *4*, 173−183.
(118) Huhn, D.; Kantner, K.; Geidel, C.; Brandholt, S.; De Cock, I.; Soenen, S. J.; Rivera Gil, P.; Montenegro, J. M.; Braeckmans, K.; Mullen, K.; Nienhaus, G. U.; Klapper, M.; Parak, W. J. Polymer-Coated Nanoparticles Interacting with Proteins and Cells: Focusing on the Sign of the Net Charge. *ACS Nano* **2013**, *7*, 3253−3263.
(119) Donahue, N. D.; Acar, H.; Wilhelm, S. Concepts of Nanoparticle Cellular Uptake, Intracellular Trafficking, and Kinetics in Nanomedicine. *Adv. Drug Delivery Rev.* **2019**, *143*, 68−96.
(120) Hao, R.; Xing, R.; Xu, Z.; Hou, Y.; Gao, S.; Sun, S. Synthesis, Functionalization, and Biomedical Applications of Multifunctional Magnetic Nanoparticles. *Adv. Mater.* **2010**, *22*, 2729−2742.
(121) Gupta, A. K.; Naregalkar, R. R.; Vaidya, V. D.; Gupta, M. Recent Advances on Surface Engineering of Magnetic Iron Oxide Nanoparticles and their Biomedical Applications. *Nanomedicine* **2007**, *2*, 23−39.
(122) Mohammed, L.; Gomaa, H. G.; Ragab, D.; Zhu, J. Magnetic Nanoparticles for Environmental and Biomedical Applications: A Review. *Particuology* **2017**, *30*, 1−14.
(123) Wagner, A. M.; Knipe, J. M.; Orive, G.; Peppas, N. A. Quantum Dots in Biomedical Applications. *Acta Biomater.* **2019**, *94*, 44−63.
(124) Abdul Jalil, R.; Zhang, Y. Biocompatibility of Silica Coated $NaYF_4$ Upconversion Fluorescent Nanocrystals. *Biomaterials* **2008**, *29*, 4122−4128.
(125) Sun, L.; Wei, R.; Feng, J.; Zhang, H. Tailored Lanthanide-Doped Upconversion Nanoparticles and their Promising Bioapplication Prospects. *Coord. Chem. Rev.* **2018**, *364*, 10−32.
(126) Gerion, D.; Pinaud, F.; Williams, S. C.; Parak, W. J.; Zanchet, D.; Weiss, S.; Alivisatos, A. P. Synthesis and Properties of Biocompatible Water-Soluble Silica-Coated CdSe/ZnS Semiconductor Quantum Dots. *J. Phys. Chem. B* **2001**, *105*, 8861−8871.
(127) Drijvers, E.; Liu, J.; Harizaj, A.; Wiesner, U.; Braeckmans, K.; Hens, Z.; Aubert, T. Efficient Endocytosis of Inorganic Nanoparticles with Zwitterionic Surface Functionalization. *ACS Appl. Mater. Interfaces* **2019**, *11*, 38475−38482.
(128) Debayle, M.; Balloul, E.; Dembele, F.; Xu, X.; Hanafi, M.; Ribot, F.; Monzel, C.; Coppey, M.; Fragola, A.; Dahan, M.; Pons, T.; Lequeux, N. Zwitterionic Polymer Ligands: An Ideal Surface Coating To Totally Suppress Protein-Nanoparticle Corona Formation? *Biomaterials* **2019**, *219*, 119357.
(129) Zhang, F.; Lees, E.; Amin, F.; Rivera Gil, P.; Yang, F.; Mulvaney, P.; Parak, W. J. Polymer-Coated Nanoparticles: A Universal Tool for Biolabelling Experiments. *Small* **2011**, *7*, 3113−3127.
(130) Bobo, D.; Robinson, K. J.; Islam, J.; Thurecht, K. J.; Corrie, S. R. Nanoparticle-Based Medicines: A Review of FDA-Approved Materials and Clinical Trials to Date. *Pharm. Res.* **2016**, *33*, 2373−2387.
(131) Karakoti, A. S.; Das, S.; Thevuthasan, S.; Seal, S. PEGylated Inorganic Nanoparticles. *Angew. Chem., Int. Ed.* **2011**, *50*, 1980−1994.
(132) Roberts, M. J.; Bentley, M. D.; Harris, J. M. Chemistry for Peptide and Protein PEGylation. *Adv. Drug Delivery Rev.* **2002**, *54*, 459−476.
(133) Shiraishi, K.; Yokoyama, M. Toxicity and Immunogenicity Concerns Related to PEGylated-Micelle Carrier Systems: A Review. *Sci. Technol. Adv. Mater.* **2019**, *20*, 324−336.
(134) Grenier, P.; Viana, I. M. O.; Lima, E. M.; Bertrand, N. Anti-Polyethylene Glycol Antibodies Alter the Protein Corona Deposited on Nanoparticles and the Physiological Pathways Regulating their Fate *in Vivo*. *J. Controlled Release* **2018**, *287*, 121−131.
(135) Carrasco, E.; del Rosal, B.; Sanz-Rodríguez, F.; de la Fuente, Á. J.; Gonzalez, P. H.; Rocha, U.; Kumar, K. U.; Jacinto, C.; Solé, J. G.; Jaque, D. Intratumoral Thermal Reading During Photo-Thermal Therapy by Multifunctional Fluorescent Nanoparticles. *Adv. Funct. Mater.* **2015**, *25*, 615−626.
(136) Lan, M.; Zhao, S.; Zhang, Z.; Yan, L.; Guo, L.; Niu, G.; Zhang, J.; Zhao, J.; Zhang, H.; Wang, P.; Zhu, G.; Lee, C.-S.; Zhang, W. Two-Photon-Excited Near-Infrared Emissive Carbon Dots as Multifunctional Agents for Fluorescence Imaging and Photothermal Therapy. *Nano Res.* **2017**, *10*, 3113−3123.
(137) Al-Jamal, W. T.; Al-Jamal, K. T.; Bomans, P. H.; Frederik, P. M.; Kostarelos, K. Functionalized-Quantum-Dot-Liposome Hybrids as Multimodal Nanoparticles for Cancer. *Small* **2008**, *4*, 1406−1415.
(138) Chen, G.; Jaskula-Sztul, R.; Esquibel, C. R.; Lou, I.; Zheng, Q.; Dammalapati, A.; Harrison, A.; Eliceiri, K. W.; Tang, W.; Chen, H.; Gong, S. Neuroendocrine Tumor-Targeted Upconversion Nanoparticle-Based Micelles for Simultaneous NIR-Controlled Combination Chemotherapy and Photodynamic Therapy, and Fluorescence Imaging. *Adv. Funct. Mater.* **2017**, *27*, 1604671.
(139) Cho, K.; Wang, X.; Nie, S.; Chen, Z. G.; Shin, D. M. Therapeutic Nanoparticles for Drug Delivery in Cancer. *Clin. Cancer Res.* **2008**, *14*, 1310−1316.

https://dx.doi.org/10.1021/acsnano.0c08349
ACS Nano 2021, 15, 1917−1941

(140) Attia, M. F.; Anton, N.; Wallyn, J.; Omran, Z.; Vandamme, T. F. An Overview of Active and Passive Targeting Strategies To Improve the Nanocarriers Efficiency to Tumour Sites. *J. Pharm. Pharmacol.* **2019**, *71*, 1185−1198.
(141) Zhong, Y.; Meng, F.; Deng, C.; Zhong, Z. Ligand-Directed Active Tumor-Targeting Polymeric Nanoparticles for Cancer Chemotherapy. *Biomacromolecules* **2014**, *15*, 1955−1969.
(142) Byrne, J. D.; Betancourt, T.; Brannon-Peppas, L. Active Targeting Schemes for Nanoparticle Systems in Cancer Therapeutics. *Adv. Drug Delivery Rev.* **2008**, *60*, 1615−1626.
(143) Tang, W.; Fan, W.; Lau, J.; Deng, L.; Shen, Z.; Chen, X. Emerging Blood-Brain-Barrier-Crossing Nanotechnology for Brain Cancer Theranostics. *Chem. Soc. Rev.* **2019**, *48*, 2967−3014.
(144) Wilhelm, S.; Tavares, A. J.; Dai, Q.; Ohta, S.; Audet, J.; Dvorak, H. F.; Chan, W. C. W. Analysis of Nanoparticle Delivery to Tumours. *Nat. Rev. Mater.* **2016**, *1*, 16014.
(145) Zhou, J.; Kroll, A. V.; Holay, M.; Fang, R. H.; Zhang, L. Biomimetic Nanotechnology toward Personalized Vaccines. *Adv. Mater.* **2020**, *32*, No. 1901255.
(146) Fontana, F.; Shahbazi, M. A.; Liu, D.; Zhang, H.; Makila, E.; Salonen, J.; Hirvonen, J. T.; Santos, H. A. Multistaged Nanovaccines Based on Porous Silicon@Acetalated Dextran@Cancer Cell Membrane for Cancer Immunotherapy. *Adv. Mater.* **2017**, *29*, 1603239.
(147) Rao, L.; Bu, L. L.; Cai, B.; Xu, J. H.; Li, A.; Zhang, W. F.; Sun, Z. J.; Guo, S. S.; Liu, W.; Wang, T. H.; Zhao, X. Z. Cancer Cell Membrane-Coated Upconversion Nanoprobes for Highly Specific Tumor Imaging. *Adv. Mater.* **2016**, *28*, 3460−3466.
(148) Rao, L.; Yu, G. T.; Meng, Q. F.; Bu, L. L.; Tian, R.; Lin, L. S.; Deng, H.; Yang, W.; Zan, M.; Ding, J.; Li, A.; Xiao, H.; Sun, Z. J.; Liu, W.; Chen, X. Cancer Cell Membrane-Coated Nanoparticles for Personalized Therapy in Patient-Derived Xenograft Models. *Adv. Funct. Mater.* **2019**, *29*, 1905671.
(149) Hu, C. M.; Fang, R. H.; Wang, K. C.; Luk, B. T.; Thamphiwatana, S.; Dehaini, D.; Nguyen, P.; Angsantikul, P.; Wen, C. H.; Kroll, A. V.; Carpenter, C.; Ramesh, M.; Qu, V.; Patel, S. H.; Zhu, J.; Shi, W.; Hofman, F. M.; Chen, T. C.; Gao, W.; Zhang, K.; et al. Nanoparticle Biointerfacing by Platelet Membrane Cloaking. *Nature* **2015**, *526*, 118−121.
(150) Hu, C. M.; Zhang, L.; Aryal, S.; Cheung, C.; Fang, R. H.; Zhang, L. Erythrocyte Membrane-Camouflaged Polymeric Nanoparticles as a Biomimetic Delivery Platform. *Proc. Natl. Acad. Sci. U. S. A.* **2011**, *108*, 10980−10985.
(151) Bros, M.; Nuhn, L.; Simon, J.; Moll, L.; Mailander, V.; Landfester, K.; Grabbe, S. The Protein Corona as a Confounding Variable of Nanoparticle-Mediated Targeted Vaccine Delivery. *Front. Immunol.* **2018**, *9*, 1760.
(152) Corbo, C.; Molinaro, R.; Parodi, A.; Toledano Furman, N. E.; Salvatore, F.; Tasciotti, E. The Impact of Nanoparticle Protein Corona on Cytotoxicity, Immunotoxicity and Target Drug Delivery. *Nanomedicine* **2016**, *11*, 81−100.
(153) Papi, M.; Caputo, D.; Palmieri, V.; Coppola, R.; Palchetti, S.; Bugli, F.; Martini, C.; Digiacomo, L.; Pozzi, D.; Caracciolo, G. Clinically Approved PEGylated Nanoparticles are Covered by a Protein Corona that Boosts the Uptake by Cancer Cells. *Nanoscale* **2017**, *9*, 10327−10334.
(154) Del Rosal, B.; Ortgies, D. H.; Fernandez, N.; Sanz-Rodriguez, F.; Jaque, D.; Rodriguez, E. M. Overcoming Autofluorescence: Long-Lifetime Infrared Nanoparticles for Time-Gated *in Vivo* Imaging. *Adv. Mater.* **2016**, *28*, 10188−10193.
(155) Yang, W.; Srivastava, P. K.; Han, S.; Jing, L.; Tu, C. C.; Chen, S. L. Optomechanical Time-Gated Fluorescence Imaging Using Long-Lived Silicon Quantum Dot Nanoparticles. *Anal. Chem.* **2019**, *91*, 5499−5503.
(156) Kodama, Y. Time Gating of Chloroplast Autofluorescence Allows Clearer Fluorescence Imaging In Planta. *PLoS One* **2016**, *11*, No. e0152484.
(157) Rubin, M. B.; Braslavsky, S. E. Quantum Yield: The Term and the Symbol. A Historical Search. *Photochem. Photobiol. Sci.* **2010**, *9*, 670−674.
(158) McNaught, A. D.; Wilkinson, A. *The IUPAC Compendium of Chemical Terminology*, 2nd ed.; Blackwell Science: Oxford, England, 1997.
(159) Johnson, N. J.; He, S.; Diao, S.; Chan, E. M.; Dai, H.; Almutairi, A. Direct Evidence for Coupled Surface and Concentration Quenching Dynamics in Lanthanide-Doped Nanocrystals. *J. Am. Chem. Soc.* **2017**, *139*, 3275−3282.
(160) Wuister, S. F.; de Mello Donega, C.; Meijerink, A. Luminescence Temperature Antiquenching of Water-Soluble CdTe Quantum Dots: Role of the Solvent. *J. Am. Chem. Soc.* **2004**, *126*, 10397−10402.
(161) Cheng, T.; Marin, R.; Skripka, A.; Vetrone, F. Small and Bright Lithium-Based Upconverting Nanoparticles. *J. Am. Chem. Soc.* **2018**, *140*, 12890−12899.
(162) Boercker, J. E.; Woodall, D. L.; Cunningham, P. D.; Placencia, D.; Ellis, C. T.; Stewart, M. H.; Brintlinger, T. H.; Stroud, R. M.; Tischler, J. G. Synthesis and Characterization of PbS/ZnS Core/Shell Nanocrystals. *Chem. Mater.* **2018**, *30*, 4112−4123.
(163) Zang, H.; Li, H.; Makarov, N. S.; Velizhanin, K. A.; Wu, K.; Park, Y. S.; Klimov, V. I. Thick-Shell CuInS2/ZnS Quantum Dots with Suppressed "Blinking" and Narrow Single-Particle Emission Line Widths. *Nano Lett.* **2017**, *17*, 1787−1795.
(164) Shen, Y.; Lifante, J.; Ximendes, E.; Santos, H. D. A.; Ruiz, D.; Juarez, B. H.; Zabala Gutierrez, I.; Torres Vera, V.; Rubio Retama, J.; Martin Rodriguez, E.; Ortgies, D. H.; Jaque, D.; Benayas, A.; Del Rosal, B. Perspectives for Ag_2S NIR-II Nanoparticles in Niomedicine: From Imaging to Multifunctionality. *Nanoscale* **2019**, *11*, 19251−19264.
(165) Jiang, L.; Ding, H.; Xu, M.; Hu, X.; Li, S.; Zhang, M.; Zhang, Q.; Wang, Q.; Lu, S.; Tian, Y.; Bi, H. Carbon Dots: UV-Vis-NIR Full-Range Responsive Carbon Dots with Large Multiphoton Absorption Cross Sections and Deep-Red Fluorescence at Nucleoli and *in Vivo*. *Small* **2020**, *16*, 2000680.
(166) Marin, R.; Brunet, G.; Murugesu, M. Shining New Light on Multifunctional Lanthanide Single-Molecule Magnets. *Angew. Chem. Int. Ed.* **2019** DOI: 10.1002/anie.201910299.
(167) Marin, R.; Jaque, D. Doping Lanthanide Ions in Colloidal Semiconductor Nanocrystals for Brighter Photoluminescence. *Chem. Rev.* **2020** DOI: 10.1021/acs.chemrev.0c00692.
(168) Marin, R.; Jaque Garcia, D.; Benayas, A. Switching to the Brighter Lane: Pathways to Boost the Absorption of Lanthanide-Doped Nanoparticles. *Nanoscale Horiz.* **2021** DOI: 10.1039/D0NH00627K.
(169) Zhang, W.; Chen, T.; Su, L.; Ge, X.; Chen, X.; Song, J.; Yang, H. Quantum Dot-Based Sensitization System for Boosted Photon Absorption and Enhanced Second Near-Infrared Luminescence of Lanthanide-Doped Nanoparticle. *Anal. Chem.* **2020**, *92*, 6094−6102.
(170) Song, D.; Chi, S.; Li, X.; Wang, C.; Li, Z.; Liu, Z. Upconversion System with Quantum Dots as Sensitizer: Improved Photoluminescence and PDT Efficiency. *ACS Appl. Mater. Interfaces* **2019**, *11*, 41100−41108.
(171) Creutz, S. E.; Fainblat, R.; Kim, Y.; De Siena, M. C.; Gamelin, D. R. A Selective Cation Exchange Strategy for the Synthesis of Colloidal Yb^{3+}-Doped Chalcogenide Nanocrystals with Strong Broadband Visible Absorption and Long-Lived Near-Infrared Emission. *J. Am. Chem. Soc.* **2017**, *139*, 11814−11824.
(172) Das, A.; Mao, C.; Cho, S.; Kim, K.; Park, W. Over 1000-Fold Enhancement of Upconversion Luminescence Using Water-Dispersible Metal-Insulator-Metal Nanostructures. *Nat. Commun.* **2018**, *9*, 4828.
(173) Ji, B.; Giovanelli, E.; Habert, B.; Spinicelli, P.; Nasilowski, M.; Xu, X.; Lequeux, N.; Hugonin, J. P.; Marquier, F.; Greffet, J. J.; Dubertret, B. Non-Blinking Quantum Dot with a Plasmonic Nanoshell Resonator. *Nat. Nanotechnol.* **2015**, *10*, 170−175.
(174) Giannini, V.; Fernandez-Dominguez, A. I.; Heck, S. C.; Maier, S. A. Plasmonic Nanoantennas: Fundamentals and their Use in Controlling the Radiative Properties of Nanoemitters. *Chem. Rev.* **2011**, *111*, 3888−3912.
(175) Smith, M.; Fork, R. L.; Cole, S. Safe Delivery of Optical Power from Space. *Opt. Express* **2001**, *8*, 537−546.

(176) Beier, H. T.; Jansen, E. D.; Thomas, R. J.; Kumru, S. S.; Schmidt, M. S.; Boretsky, A. R.; Tijerina, A. J.; Shingledecker, A. D.; Noojin, G. D.; Peterson, A. M.; DeLisi, M. P. Porcine Skin Damage Thresholds for Pulsed Nanosecond-Scale Laser Exposure at 1064 nm. In *Optical Interactions with Tissue and Cells XXIX*; Bennett, L. I., Ed.; SPIE: Bellingham, WA, 2020; Vol. *10492*, pp 112380C.
(177) Frenz, M.; Mischler, C.; Romano, V.; Forrer, M.; Mller, O. M.; Weber, H. P. Effect of Mechanical Tissue Properties on Thermal Damage in Skin After IR-Laser Ablation. *Appl. Phys. B: Photophys. Laser Chem.* **1991**, *52*, 251−258.
(178) Ghanmi, A.; Abbas, I. A. An Analytical Study on the Fractional Transient Heating Within the Skin Tissue During the Thermal Therapy. *J. Therm. Biol.* **2019**, *82*, 229−233.
(179) Golovynskyi, S.; Golovynska, I.; Stepanova, L. I.; Datsenko, O. I.; Liu, L.; Qu, J.; Ohulchanskyy, T. Y. Optical Windows for Head Tissues in Near-Infrared and Short-Wave Infrared Regions: Approaching Transcranial Light Applications. *J. Biophotonics* **2018**, *11*, No. e201800141.
(180) Wang, M.; Wu, C.; Sinefeld, D.; Li, B.; Xia, F.; Xu, C. Comparing the Effective Attenuation Lengths for Long Wavelength *in Vivo* Imaging of the Mouse Brain. *Biomed. Opt. Express* **2018**, *9*, 3534−3543.
(181) Cheong, W. F.; Prahl, S. A.; Welch, A. J. A Review of the Optical Properties of Biological Tissues. *IEEE J. Quantum Electron.* **1990**, *26*, 2166−2185.
(182) Smith, A. M.; Mancini, M. C.; Nie, S. Bioimaging: Second Window for *in Vivo* Imaging. *Nat. Nanotechnol.* **2009**, *4*, 710−711.
(183) Wang, V. W.; Wu, H.-I. *Biomedical Optics: Principles and Imaging*; Wiley: Hoboken, NJ, 2007.
(184) Yaroslavsky, A. N.; Schulze, P. C.; Yaroslavsky, I. V.; Schober, R.; Ulrich, F.; Schwarzmaier, H. J. Optical Properties of Selected Native and Coagulated Human Brain Tissues *in Vitro* in the Visible and Near Infrared Spectral Range. *Phys. Med. Biol.* **2002**, *47*, 2059−2073.
(185) Nyk, M.; Kumar, R.; Ohulchanskyy, T. Y.; Bergey, E. J.; Prasad, P. N. High Contrast *in Vitro* and *in Vivo* Photoluminescence Bioimaging Using Near Infrared to Near Infrared Up-Conversion in Tm^{3+} and Yb^{3+} Doped Fluoride Nanophosphors. *Nano Lett.* **2008**, *8*, 3834−3838.
(186) Bashkatov, A. N.; Genina, E. A.; Tuchin, V. V. Optical Properties of Skin, Subcutaneous, and Muscle Tissues: A Review. *J. Innovative Opt. Health Sci.* **2011**, *04*, 9−38.
(187) Tozer, B. A. The Calculation of Maximum Permissible Exposure Levels for Laser Radiation. *J. Phys. E: Sci. Instrum.* **1979**, *12*, 922−922.
(188) Yang, K.; Zhang, S.; Zhang, G.; Sun, X.; Lee, S. T.; Liu, Z. Graphene in Mice: Ultrahigh *in Vivo* Tumor Uptake and Efficient Photothermal Therapy. *Nano Lett.* **2010**, *10*, 3318−3323.
(189) Ximendes, E. C.; Rocha, U.; Jacinto, C.; Kumar, K. U.; Bravo, D.; Lopez, F. J.; Rodriguez, E. M.; Garcia-Sole, J.; Jaque, D. Self-Monitored Photothermal Nanoparticles Based on Core-Shell Engineering. *Nanoscale* **2016**, *8*, 3057−3066.
(190) Ximendes, E. C.; Santos, W. Q.; Rocha, U.; Kagola, U. K.; Sanz-Rodriguez, F.; Fernandez, N.; Gouveia-Neto, A. d. S.; Bravo, D.; Domingo, A. M.; del Rosal, B.; Brites, C. D. S.; Carlos, L. D.; Jaque, D.; Jacinto, C. Unveiling *in Vivo* Subcutaneous Thermal Dynamics by Infrared Luminescent Nanothermometers. *Nano Lett.* **2016**, *16*, 1695−1703.
(191) Li, X.; Jiang, M.; Li, Y.; Xue, Z.; Zeng, S.; Liu, H. 808nm Laser-Triggered NIR-II Emissive Rare-Earth Nanoprobes for Small Tumor Detection and Blood Vessel Imaging. *Mater. Sci. Eng., C* **2019**, *100*, 260−268.
(192) Communal, J.-E. Comparing Camera Sensitivity with Noise Equivalent Irradiance. *In 2014 6th Workshop on Hyperspectral Image and Signal Processing: Evolution in Remote Sensing (WHISPERS)* **2014**, 1−4.
(193) Swartling, J.; Dam, J. S.; Andersson-Engels, S. Comparison of Spatially and Temporally Resolved Diffuse-Reflectance Measurement Systems for Determination of Biomedical Optical Properties. *Appl. Opt.* **2003**, *42*, 4612−4620.
(194) Svensson, T.; Swartling, J.; Taroni, P.; Torricelli, A.; Lindblom, P.; Ingvar, C.; Andersson-Engels, S. Characterization of Normal Breast Tissue Heterogeneity Using Time-Resolved Near-Infrared Spectroscopy. *Phys. Med. Biol.* **2005**, *50*, 2559−2571.
(195) Tromberg, B. J.; Shah, N.; Lanning, R.; Cerussi, A.; Espinoza, J.; Pham, T.; Svaasand, L.; Butler, J. Non-Invasive *in Vivo* Characterization of Breast Tumors Using Photon Migration Spectroscopy. *Neoplasia* **2000**, *2*, 26−40.
(196) Tromberg, B. J.; Coquoz, O.; Fishkin, J. B.; Pham, T.; Anderson, E. R.; Butler, J.; Cahn, M.; Gross, J. D.; Venugopalan, V.; Pham, D. Non-Invasive Measurements of Breast Tissue Optical Properties Using Frequency-Domain Photon Migration. *Philos. Trans. R. Soc., B* **1997**, *352*, 661−668.
(197) Bays, R.; Wagnières, G.; Robert, D.; Braichotte, D.; Savary, J.-F.; Monnier, P.; van den Bergh, H. Clinical Determination of Tissue Optical Properties by Endoscopic Spatially Resolved Reflectometry. *Appl. Opt.* **1996**, *35*, 1756−1766.
(198) Doornbos, R. M.; Lang, R.; Aalders, M. C.; Cross, F. W.; Sterenborg, H. J. The Determination of *in Vivo* Human Tissue Optical Properties and Absolute Chromophore Concentrations Using Spatially Resolved Steady-State Diffuse Reflectance Spectroscopy. *Phys. Med. Biol.* **1999**, *44*, 967−981.
(199) Pilz, M.; Honold, S.; Kienle, A. Determination of the Optical Properties of Turbid Media by Measurements of the Spatially Resolved Reflectance Considering the Point-Spread Function of the Camera System. *J. Biomed. Opt.* **2008**, *13*, 054047.
(200) Azzi, L.; El-Alfy, M.; Martel, C.; Labrie, F. Gender Differences in Mouse Skin Morphology and Specific Effects of Sex Steroids and Dehydroepiandrosterone. *J. Invest. Dermatol.* **2005**, *124*, 22−27.
(201) Kowalewska, P. M.; Margetts, P. J.; Fox-Robichaud, A. E. Peritoneal Dialysis Catheter Increases Leukocyte Recruitment in the Mouse Parietal Peritoneum Microcirculation and Causes Fibrosis. *Peritoneal Dial. Int.* **2016**, *36*, 7−15.
(202) Richardson, L.; Venkataraman, S.; Stevenson, P.; Yang, Y.; Moss, J.; Graham, L.; Burton, N.; Hill, B.; Rao, J.; Baldock, R. A.; Armit, C. EMAGE Mouse Embryo Spatial Gene Expression Database: 2014 Update. *Nucleic Acids Res.* **2014**, *42*, D835−D844.
(203) Diot, G.; Metz, S.; Noske, A.; Liapis, E.; Schroeder, B.; Ovsepian, S. V.; Meier, R.; Rummeny, E.; Ntziachristos, V. Multispectral Optoacoustic Tomography (MSOT) of Human Breast Cancer. *Clin. Cancer Res.* **2017**, *23*, 6912−6922.
(204) Li, L.; Cazzell, M.; Babawale, O.; Liu, H. Automated Voxel Classification Used With Atlas-Guided Diffuse Optical Tomography for Assessment of Functional Brain Networks in Young and Older Adults. *Neurophotonics* **2016**, *3*, 045002.
(205) Bosschaart, N.; Leproux, A.; Abdalsalam, O.; Chen, W. P.; McLaren, C. E.; Tromberg, B. J.; O'Sullivan, T. D. Diffuse Optical Spectroscopic Imaging for the Investigation of Human Lactation Physiology: A Case Study on Mammary Involution. *J. Biomed. Opt.* **2019**, *24* (5), 1−8.
(206) Hu, G.; Zhang, Q.; Ivkovic, V.; Strangman, G. E. Ambulatory Diffuse Optical Tomography and Multimodality Physiological Monitoring System for Muscle and Exercise Applications. *J. Biomed. Opt.* **2016**, *21*, 091314.
(207) Lighter, D.; Hughes, J.; Styles, I.; Filer, A.; Dehghani, H. Multispectral, Non-Contact Diffuse Optical Tomography of Healthy Human Finger Joints. *Biomed. Opt. Express* **2018**, *9*, 1445−1460.
(208) Konugolu Venkata Sekar, S.; Pagliazzi, M.; Negredo, E.; Martelli, F.; Farina, A.; Dalla Mora, A.; Lindner, C.; Farzam, P.; Perez-Alvarez, N.; Puig, J.; Taroni, P.; Pifferi, A.; Durduran, T. *In Vivo*, Non-Invasive Characterization of Human Bone by Hybrid Broadband (600−1200 nm) Diffuse Optical and Correlation Spectroscopies. *PLoS One* **2016**, *11*, No. e0168426.
(209) Peelle, J. E. Optical Neuroimaging of Spoken Language. *Lang. Cogn. Neurosci.* **2017**, *32*, 847−854.
(210) Lee, C. W.; Cooper, R. J.; Austin, T. Diffuse Optical Tomography To Investigate the Newborn Brain. *Pediatr. Res.* **2017**, *82*, 376−386.
(211) Zhu, Q.; Ricci, A., Jr; Hegde, P.; Kane, M.; Cronin, E.; Merkulov, A.; Xu, Y.; Tavakoli, B.; Tannenbaum, S. Assessment of Functional Differences in Malignant and Benign Breast Lesions and

https://dx.doi.org/10.1021/acsnano.0c08349
ACS Nano 2021, 15, 1917−1941

Improvement of Diagnostic Accuracy by Using US-guided Diffuse Optical Tomography in Conjunction with Conventional US. *Radiology* **2016**, *280*, 387−397.
(212) Fishell, A. K.; Burns-Yocum, T. M.; Bergonzi, K. M.; Eggebrecht, A. T.; Culver, J. P. Mapping Brain Function During Naturalistic Viewing Using High-Density Diffuse Optical Tomography. *Sci. Rep.* **2019**, *9*, 11115.
(213) Chalia, M.; Dempsey, L. A.; Cooper, R. J.; Lee, C. W.; Gibson, A. P.; Hebden, J. C.; Austin, T. Diffuse Optical Tomography for the Detection of Perinatal Stroke at the Cot Side: A Pilot Study. *Pediatr. Res.* **2019**, *85*, 1001−1007.
(214) Ackerman, M. J. The Visible Human Project. *Proc. IEEE* **1998**, *86*, 504−511.
(215) Ackerman, M. J. The Visible Human Project®: From Body to Bits. *Conf. Proc. IEEE Eng. Med. Biol. Soc.* **2016**, *2016*, 3338−3341.
(216) Tuchin, V. V.; Bashkatov, A. N.; Genina, E. A.; Kochubey, V. I.; Tuchin, V. V. Optical Properties of Human Cranial Bone in the Spectral Range from 800 to 2000 nm. In *Saratov Fall Meeting 2005: Optical Technologies in Biophysics and Medicine VII*; Tuchin, V. V., Ed.; SPIE: Bellingham, WA, 2006; Vol. *6163*, pp 616310−616311.
(217) Oraevsky, A. A.; Sikorski, Z.; Wang, L. V.; Furmanczyk, M.; Przekwas, A. J. Modeling of Photon Migration in the Human Lung Using a Finite Volume Solver. *Proc. SPIE* **2006**, 60861Z.
(218) Choi, B.; Kollias, N.; Zeng, H.; Kang, H. W.; Wong, B. J. F.; Ilgner, J. F.; Tearney, G. J.; Gregory, K. W.; Marcu, L.; Skala, M. C.; Campagnola, P. J.; Mandelis, A.; Morris, M. D.; Sordillo, D. C.; Sordillo, L. A.; Sordillo, P. P.; Alfano, R. R. Fourth Near-Infrared Optical Window for Assessment of Bone and Other Tissues. *Proc. SPIE* **2016**, 96894J.
(219) Nogueira, M. S.; Lacerenza, M.; Sekar, S. K. V.; Buttafava, M.; Pifferi, A.; Tosi, A.; Contini, D.; Andersson-Engels, S. Broadband Extraction of Tissue Optical Properties Using a Portable Hybrid Time-Resolved Continuous Wave Instrumentation: Characterization of *ex Vivo* Organs. In *Biophotonics Congress: Biomedical Optics 2020 (Translational, Microscopy, OCT, OTS, BRAIN)*; Optical Society of America: Washington, DC, 2020.
(220) Bashkatov, A. N.; Berezin, K. V.; Dvoretskiy, K. N.; Chernavina, M. L.; Genina, E. A.; Genin, V. D.; Kochubey, V. I.; Lazareva, E. N.; Pravdin, A. B.; Shvachkina, M. E.; Timoshina, P. A.; Tuchina, D. K.; Yakovlev, D. D.; Yakovlev, D. A.; Yanina, I. Y.; Zhernovaya, O. S.; Tuchin, V. V. Measurement of Tissue Optical Properties in the Context of Tissue Optical Clearing. *J. Biomed. Opt.* **2018**, *23*, 091416.
(221) Cubeddu, R.; D'Andrea, C.; Pifferi, A.; Taroni, P.; Torricelli, A.; Valentini, G. Effects of the Menstrual Cycle on the Red and Near-Infrared Optical Properties of the Human Breast. *Photochem. Photobiol.* **2000**, *72*, 383−391.
(222) Genina, E. A.; Derbov, V. L.; Meglinski, I.; Tuchin, V. V.; Kozintseva, M. D.; Bashkatov, A. N.; Kochubey, V. I.; Genina, E. A.; Gorodkov, S. Y.; Morozov, D. A.; Tuchin, V. V. Optical Properties of Parietal Peritoneum in the Spectral Range 350−2500 nm. In *Saratov Fall Meeting 2013: Optical Technologies in Biophysics and Medicine XV; and Laser Physics and Photonics XV*; SPIE: Bellingham, WA, 2014; Vol. *9031*.
(223) Tuchin, V. V.; Bashkatov, A. N.; Genina, E. A.; Kochubey, V. I.; Gavrilova, A. A.; Kapralov, S. V.; Grishaev, V. A.; Tuchin, V. V. Optical Properties of Human Stomach Mucosa in the Spectral Range from 400 to 2000 nm. *Biomed. Laser: Technol. Clin. Appl.* **2007**, *22*, 95−104.
(224) Germer, C.-T.; Roggan, A.; Ritz, J. P.; Isbert, C.; Albrecht, D.; Müller, G.; Buhr, H. J. Optical Properties of Native and Coagulated Human Liver Tissue and Liver Metastases in the Near Infrared Range. *Lasers Surg. Med.* **1998**, *23*, 194−203.
(225) Ntziachristos, V.; Ripoll, J.; Weissleder, R. Would Near-Infrared Fluorescence Signals Propagate Through Large Human Organs for Clinical Studies? *Opt. Lett.* **2002**, *27*, 333−335.
(226) Ozsahin, I.; Gharagouzloo, C.; Belov, V.; Alpert, N.; Fakhri, G. Awake Animal Functional Imaging To Investigate the Effects of General Anesthesia on Brain. Proceedings from the *2018 Advances in Science and Engineering Technology International Conferences (ASET)*, February 6, 2018, Abu Dhabi, UAE; IEEE: New York, 2018.
(227) Heinke, W.; Koelsch, S. *Curr. Opin. Anaesthesiol.* **2005**, *18*, 625−631.
(228) Alkire, M. T.; Haier, R. J.; Barker, S. J.; Shah, N. K.; Wu, J. C.; Kao, Y. J. Cerebral Metabolism During Propofol Anesthesia in Humans Studied with Positron Emission Tomography. *Anesthesiology* **1995**, *82*, 393−403.
(229) Park, K.; Chen, W.; Volkow, N. D.; Allen, C. P.; Pan, Y.; Du, C. Hemodynamic and Neuronal Responses to Cocaine Differ in Awake *versus* Anesthetized Animals: Optical Brain Imaging Study. *NeuroImage* **2019**, *188*, 188−197.
(230) Kyme, A. Z.; Angelis, G. I.; Eisenhuth, J.; Fulton, R. R.; Zhou, V.; Hart, G.; Popovic, K.; Akhtar, M.; Ryder, W. J.; Clemens, K. J.; Balleine, B. W.; Parmar, A.; Pascali, G.; Perkins, G.; Meikle, S. R. Open-Field PET: Simultaneous Brain Functional Imaging and Behavioural Response Measurements in Freely Moving Small Animals. *NeuroImage* **2019**, *188*, 92−101.
(231) Nath, T.; Mathis, A.; Chen, A. C.; Patel, A.; Bethge, M.; Mathis, M. W. Using DeepLabCut for 3D Markerless Pose Estimation Across Species and Behaviors. *Nat. Protoc.* **2019**, *14*, 2152−2176.
(232) Han, J.; Jentzen, A.; E, W. Solving High-Dimensional Partial Differential Equations Using Deep Learning. *Proc. Natl. Acad. Sci. U. S. A.* **2018**, *115*, 8505−8510.
(233) Würfl, T.; Ghesu, F. C.; Christlein, V.; Maier, A. Deep Learning Computed Tomography. *In Medical Image Computing and Computer-Assisted Intervention - MICCAI 2016* **2016**, *9902*, 432−440.
(234) Lee, H.; Huang, C.; Yune, S.; Tajmir, S. H.; Kim, M.; Do, S. Machine Friendly Machine Learning: Interpretation of Computed Tomography Without Image Reconstruction. *Sci. Rep.* **2019**, *9*, 15540.
(235) Dong, J.; Fu, J.; He, Z. A Deep Learning Reconstruction Framework for X-Ray Computed Tomography with Incomplete Data. *PLoS One* **2019**, *14*, No. e0224426.
(236) Chen, H.; Zhang, Y.; Kalra, M. K.; Lin, F.; Chen, Y.; Liao, P.; Zhou, J.; Wang, G. Low-Dose CT With a Residual Encoder-Decoder Convolutional Neural Network. *IEEE Trans. Med. Imaging* **2017**, *36*, 2524−2535.
(237) Schlemper, J.; Caballero, J.; Hajnal, J. V.; Price, A.; Rueckert, D. In *A Deep Cascade of Convolutional Neural Networks for MR Image Reconstruction*; Springer International Publishing: Cham, 2017; pp 647−658.
(238) McCann, M. T.; Jin, K. H.; Unser, M. Convolutional Neural Networks for Inverse Problems in Imaging: A Review. *IEEE Signal Process. Mag.* **2017**, *34*, 85−95.
(239) Yoo, J.; Sabir, S.; Heo, D.; Kim, K. H.; Wahab, A.; Choi, Y.; Lee, S. I.; Chae, E. Y.; Kim, H. H.; Bae, Y. M.; Choi, Y. W.; Cho, S.; Ye, J. C. Deep Learning Diffuse Optical Tomography. *IEEE Trans. Med. Imaging* **2020**, *39*, 877−887.
(240) Ben Yedder, H.; BenTaieb, A.; Shokoufi, M.; Zahiremami, A.; Golnaraghi, F.; Hamarneh, G. In *Deep Learning Based Image Reconstruction for Diffuse Optical Tomography*; Springer International Publishing: Cham, 2018; pp 112−119.
(241) Granda, J. M.; Donina, L.; Dragone, V.; Long, D. L.; Cronin, L. Controlling an Organic Synthesis Robot with Machine Learning To Search for New Reactivity. *Nature* **2018**, *559*, 377−381.
(242) Li, Z.; Najeeb, M. A.; Alves, L.; Sherman, A. Z.; Shekar, V.; Cruz Parrilla, P.; Pendleton, I. M.; Wang, W.; Nega, P. W.; Zeller, M.; Schrier, J.; Norquist, A. J.; Chan, E. M. Robot-Accelerated Perovskite Investigation and Discovery. *Chem. Mater.* **2020**, *32*, 5650−5663.
(243) Flusberg, B. A.; Cocker, E. D.; Piyawattanametha, W.; Jung, J. C.; Cheung, E. L.; Schnitzer, M. J. Fiber-Optic Fluorescence Imaging. *Nat. Methods* **2005**, *2*, 941−950.
(244) Andersson-Engels, S.; Klinteberg, C.; Svanberg, K.; Svanberg, S. *In Vivo* Fluorescence Imaging for Tissue Diagnostics. *Phys. Med. Biol.* **1997**, *42*, 815−824.
(245) Zeng, H.; Weiss, A.; Cline, R.; MacAulay, C. E. Real-Time Endoscopic Fluorescence Imaging for Early Cancer Detection in the Gastrointestinal Tract. *Bioimaging* **1998**, *6*, 151−165.
(246) Plante, M.; Touhami, O.; Trinh, X. B.; Renaud, M. C.; Sebastianelli, A.; Grondin, K.; Gregoire, J. Sentinel Node Mapping with Indocyanine Green and Endoscopic Near-Infrared Fluorescence

https://dx.doi.org/10.1021/acsnano.0c08349
ACS Nano 2021, 15, 1917−1941

Imaging in Endometrial Cancer. A Pilot Study and Review of the Literature. *Gynecol. Oncol.* **2015**, *137*, 443−447.
(247) Papayan, G.; Akopov, A. Potential of Indocyanine Green Near-Infrared Fluorescence Imaging in Experimental and Clinical Practice. *Photodiagn. Photodyn. Ther.* **2018**, *24*, 292−299.
(248) Tsuruki, E. S.; Saito, Y.; Abe, S.; Takamaru, H.; Yamada, M.; Sakamoto, T.; Nakajima, T.; Matsuda, T.; Sekine, S.; Taniguchi, H. Evaluating the Efficacy and Safety of a Novel Endoscopic Fluorescence Imaging Modality Using Oral 5-Aminolevulinic Acid for Colorectal Tumors. *Endosc. Int. Open.* **2016**, *4*, E30−E35.
(249) Vahrmeijer, A. L.; Hutteman, M.; van der Vorst, J. R.; van de Velde, C. J.; Frangioni, J. V. Image-Guided Cancer Surgery Using Near-Infrared Fluorescence. *Nat. Rev. Clin. Oncol.* **2013**, *10*, 507−518.
(250) Weissleder, R.; Pittet, M. J. Imaging in the Era of Molecular Oncology. *Nature* **2008**, *452*, 580−589.
(251) Zhang, R. R.; Schroeder, A. B.; Grudzinski, J. J.; Rosenthal, E. L.; Warram, J. M.; Pinchuk, A. N.; Eliceiri, K. W.; Kuo, J. S.; Weichert, J. P. Beyond the Margins: Real-Time Detection of Cancer Using Targeted Fluorophores. *Nat. Rev. Clin. Oncol.* **2017**, *14*, 347−364.
(252) Ntziachristos, V. Going Deeper than Microscopy: The Optical Imaging Frontier in Biology. *Nat. Methods* **2010**, *7*, 603−614.
(253) Helmchen, F.; Denk, W. Deep Tissue Two-Photon Microscopy. *Nat. Methods* **2005**, *2*, 932−940.
(254) Wang, L. V. Multiscale Photoacoustic Microscopy and Computed Tomography. *Nat. Photonics* **2009**, *3*, 503−509.
(255) Nguyen, Q. T.; Tsien, R. Y. Fluorescence-Guided Surgery with Live Molecular Navigation—A New Cutting Edge. *Nat. Rev. Cancer* **2013**, *13*, 653−662.
(256) Park, Y.; Jeong, S.; Kim, S. Medically Translatable Quantum Dots for Biosensing and Imaging. *J. Photochem. Photobiol., C* **2017**, *30*, 51−70.
(257) Resch-Genger, U.; Grabolle, M.; Cavaliere-Jaricot, S.; Nitschke, R.; Nann, T. Quantum Dots *versus* Organic Dyes as Fluorescent Labels. *Nat. Methods* **2008**, *5*, 763−775.
(258) Probst, C. E.; Zrazhevskiy, P.; Bagalkot, V.; Gao, X. Quantum Dots as a Platform for Nanoparticle Drug Delivery Vehicle Design. *Adv. Drug Delivery Rev.* **2013**, *65*, 703−718.
(259) Hildebrandt, N.; Spillmann, C. M.; Algar, W. R.; Pons, T.; Stewart, M. H.; Oh, E.; Susumu, K.; Diaz, S. A.; Delehanty, J. B.; Medintz, I. L. Energy Transfer with Semiconductor Quantum Dot Bioconjugates: A Versatile Platform for Biosensing, Energy Harvesting, and Other Developing Applications. *Chem. Rev.* **2017**, *117*, 536−711.
(260) Zhou, J.; Yang, Y.; Zhang, C. Y. Toward Biocompatible Semiconductor Quantum Dots: From Biosynthesis and Bioconjugation to Biomedical Application. *Chem. Rev.* **2015**, *115*, 11669−11717.
(261) Wegner, K. D.; Hildebrandt, N. Quantum Dots: Bright and Versatile *in Vitro* and *in Vivo* Fluorescence Imaging Biosensors. *Chem. Soc. Rev.* **2015**, *44*, 4792−4834.

https://dx.doi.org/10.1021/acsnano.0c08349
ACS Nano 2021, 15, 1917−1941